nature mental health

Article

https://doi.org/10.1038/s44220-023-00024-0

Neuroimaging biomarkers define neurophysiological subtypes with distinct trajectories in schizophrenia

Received: 28 May 2022

Accepted: 23 January 2023

Published online: 22 March 2023

Check for updates

Yuchao Jiang[1,2,33], Jijun Wang[3,33], Enpeng Zhou[4,33], Lena Palaniyappan[5,6,7], Cheng Luo[8,9,10], Gongjun Ji[11], Jie Yang[12], Yingchan Wang[3], Yuyanan Zhang[4], Chu-Chung Huang[13,14], Shih-Jen Tsai[15], Xiao Chang[1,2], Chao Xie[1,2], Wei Zhang[1,2], Jinchao Lv[1,2], Di Chen[1,2], Chun Shen[1,2], Xinran Wu[1,2], Bei Zhang[1,2], Nanyu Kuang[1,2], Yun-Jun Sun[1,2], Jujiao Kang[1,2], Jie Zhang[1,2], Huan Huang[8], Hui He[8], Mingjun Duan[8], Yingying Tang[3], Tianhong Zhang[3], Chunbo Li[3], Xin Yu[4], Tianmei Si[4], Weihua Yue[4,16,17], Zhening Liu[12], Long-Biao Cui[18], Kai Wang[19,20,21,22,23], Jingliang Cheng[24], Ching-Po Lin[25], Dezhong Yao[8,9,10], Wei Cheng[1,2,26,27,28], Jianfeng Feng[1,2,28,29,30,31,32] & the ZIB Consortium*

Technical developments and improved access to neuroimaging techniques have brought us closer to understanding the neuropathological origins of schizophrenia. Using data-driven disease-progression modelling on cross-sectional magnetic resonance imaging (MRI) from 1,124 patients with schizophrenia, we characterize two distinct but stable 'trajectories' of brain atrophy, separately beginning in the Broca's area (subtype1) and the hippocampus (subtype2). The two trajectories are replicated in cross-validation samples. Individuals within each subtype are further classified into two stages ('pre-atrophy' and 'post-atrophy'). These subtypes show different atrophy patterns and symptom profiles. Longitudinal data from 523 patients with schizophrenia treated by antipsychotics only or adjunct transcranial magnetic stimulation (TMS) reveal that antipsychotics-only effects relate to phenotypic subtype (more effective in the subtype1) while adjunct transcranial-magnetic-stimulation effects relate to the stage (superior outcomes in the pre-atrophy stage). These findings suggest distinct pathophysiological processes underlying schizophrenia that potentially yield to stratification and prognostication—a key requirement for personalizing treatments in enduring illnesses.

Schizophrenia is a highly disabling psychiatric disorder with a lifetime prevalence of 1%, affecting about 26 million people worldwide[1]. The pathophysiological basis of schizophrenia is unclear, but more than one mechanism is suspected to play a role, given the substantial heterogeneity in clinical course[2], treatment efficacy[3] and the levels of putative biological markers[4,5]. Given this unsolved heterogeneity, currently available treatments cannot be matched to pathophysiological pathways, leading to limited long-term benefits. For more than a century, attempts have been made for clinical subtyping based on signs and symptoms[6], but this has been either unreliable or of limited

A full list of affiliations appears at the end of the paper. e-mail: wcheng@fudan.edu.cn; jffeng@fudan.edu.cn

therapeutic utility[7]. Biological stratification that maps on prognostic trajectories is urgently needed to promote individualized treatment decisions in schizophrenia.

At a group level, individuals with schizophrenia display compromised brain structure characterized by ventricular enlargement, cortical thinning and reduced subcortical volumes in the thalamus, hippocampus and amygdala[8,9], with notable worsening of these structural aberrations being reported in the early stages[10]. However, substantial inter-individual differences exist among individuals with schizophrenia, with no consistent abnormalities at an individual level, evident in radiological examinations[5,11]. These inter-individual differences in brain structure result from two distinct sources of variation: first, mechanistic differences that result in subtly different clinical features (mechanistic heterogeneity) and second, relative differences between individuals in the stage of dynamic progression (temporal heterogeneity). For example, progressive reductions in grey-matter volume (GMV) are associated with longer disease duration in schizophrenia[12]. Degree of cortical thinning is linked with different illness stages[13]. First-episode patients with schizophrenia showed subtle cortical thinning mainly in frontotemporal lobes[14], whereas chronic patients showed pronounced reductions spread across the parietal and occipital cortices[13]. Furthermore, brain atrophy associated with a range of clinical syndromes in schizophrenia has also been postulated to uncover underlying distinct pathophysiological processes[15,16]. Altogether, this evidence suggests that the complex pathological progress of schizophrenia may not be explained by a single unifying pathophysiological process but by a multitude of partially independent pathophysiological profiles. Hence, a systematic characterization of brain-atrophy progression, which accounts for variability on an individual level, is an urgent need.

Machine-learning approaches are increasingly used to parse the heterogeneous features of mental disorders[17–20]. Of these, unsupervised clustering techniques and semi-supervised methods, such as heterogeneity through discriminative analysis[21], provide powerful tools for disease subtyping[17–19,22]. In schizophrenia, previous subtyping studies have focused exclusively on either phenotypic heterogeneity[23,24] (individuals are clustered into distinct subgroups without considering disease stage) or temporal heterogeneity[13,25] (individuals are in different stages of disease progression without subtype differences), but not both. A new data-driven disease-progression model named Subtype and Stage Inference (SuStaIn), that requires only cross-sectional data, was proposed to identify subtypes with common patterns of disease progression and achieve individualized inference[26]. Using SuStaIn, a recent neuroimaging study successfully detected four distinct 'trajectories' of tau deposition in Alzheimer disease[27].

This work investigated a systematic characterization of heterogeneity in brain-atrophy patterning using structural magnetic resonance imaging (MRI) from 1,124 patients with schizophrenia (Supplementary Table 1). The aims (Extended Data Fig. 1) were (1) to identify distinct trajectories of brain atrophy in schizophrenia using SuStaIn and assign individuals to biological subtypes on the basis of their atrophy patterning, (2) to examine the associations of specific subtypes with clinical symptoms and (3) to examine treatment response to antipsychotic medication (APM) and transcranial magnetic stimulation (TMS) in subtypes. Supplementary Fig. 2 provides a flow of statistical analyses. Such brain subtyping may provide meaningful insights into the putative pathophysiological mechanisms in subsets of patients with schizophrenia. Ultimately, accurate stratification of this enduring illness requires addressing both temporal and phenotypic heterogeneity; if successful, this approach may inform designing clinical trials differently in the future.

Results

Two distinct pathophysiological pathways of brain atrophy

Using twofold cross-validation, the optimal clusters were determined at $k = 2$ (Supplementary Figs. 3–5), indicating two distinct trajectories of pathophysiological progression in schizophrenia (Fig. 1b). Regional volume loss at each stage for each subtype is visualized in Fig. 1c, which shows a progressive pattern of spatial extension that is distinct for each trajectory. Briefly, trajectory 1 exhibited a cortical-predominant phenotype (cortical primacy) where atrophy began in the Broca's area while trajectory 2 exhibited a subcortical-predominant phenotype (subcortical primacy) where atrophy began in the hippocampus (Fig. 1b and Supplementary Tables 5 and 6). Supplementary Fig. 7 also displays the trajectories of cortex and subcortex across SuStaIn stages. The differences of trajectories of atrophy in specific brain regions highlight potential phenotypic heterogeneity, suggesting there may be two different neuropathological pathways with distinct sites of origin in schizophrenia.

Stability of SuStaIn subtypes

Cross-validation shows that the pathophysiological progression of GMV changes in the two subtypes are reproducible. This reveals a high consistency of the observed trajectory (Supplementary Fig. 4) and SuStaIn stability for the individual subtyping using different features (Supplementary Method 6).

Subtype-specific atrophy patterns

By disentangling both temporal heterogeneity and phenotypic heterogeneity, we further defined four subtypes (Fig. 2a). A total of 631 (56.1%) patients with schizophrenia were assigned to trajectory 1 and further classified into two phases: 'pre-atrophy' ($S1_{pre}$, $n = 259$) or 'post-atrophy' ($S1_{post}$, $n = 372$). The remaining 593 patients (43.9%) were assigned to trajectory 2 with pre-atrophy ($S2_{pre}$, $n = 212$) and post-atrophy ($S2_{post}$, $n = 281$). The z scores of GMV images were mapped to a glass brain template for visualization of atrophy patterns in each subtype (Fig. 2a). Comparisons of region-of-interest (ROI)-wise z scores between $S1_{post}$ and $S2_{post}$ showed significantly higher z scores of cortical regions and significantly lower z scores of subcortical regions in $S1_{post}$ compared with $S2_{post}$ ($P < 0.001$, Bonferroni correction) (Fig. 2b). In addition, comparisons between subtypes ($S1_{pre}$ versus $S2_{pre}$, S1 versus S2) are shown in Supplementary Fig. 8. These results indicated more cortical reductions in subtype1 and more subcortical reductions in subtype2.

Longitudinal examination of SuStaIn trajectories

In the preceding analyses, we used SuStaIn on cross-sectional individual MRI data to make pseudo-longitudinal inferences about the pathophysiological trajectories of brain atrophy. To verify the findings, we collected longitudinal samples from our previous study[14] that included a total of 127 individuals who were drug-naive first-episode schizophrenia (FES) and scanned MRI at both baseline and 12 weeks follow-up (Supplementary Methods 7). Longitudinal data show that the fastest GMV reduction in Broca's area and the insula occured in the $S1_{pre}$ (patients with schizophrenia whose baseline GMV belongs to the earliest stage of trajectory 1 (before stage I)) (Supplementary Fig. 9). On the other hand, the fastest GMV reduction occurred in the hippocampus for the $S2_{pre}$ individuals (their baseline GMV belongs to the earliest stage of trajectory 2) (Supplementary Fig. 9). These findings are consistent with the expectation that these $S1_{pre}$/$S2_{pre}$ individuals were going from before stage I to stage I. Remarkably, mirroring the cross-sectional findings, the longitudinal observations support the concept of SuStaIn trajectories, mainly in the early part of the trajectory of brain atrophy in schizophrenia.

Relationships between regional atrophy and clinical symptoms

We examined the relationships between regional atrophy and clinical symptoms for each subtype. As expected, a higher z score of GMV (more reduction of GMV) was positively associated with an increasing Positive and Negative Syndrome Scale (PANSS) negative subscale score (worse negative symptoms) in many cortical, subcortical and cerebellar regions (Extended Data Fig. 2 and Supplementary Tables 7 and 8). Negative relationships among GMV z scores, positive symptoms and

https://doi.org/10.1038/s44220-023-00024-0

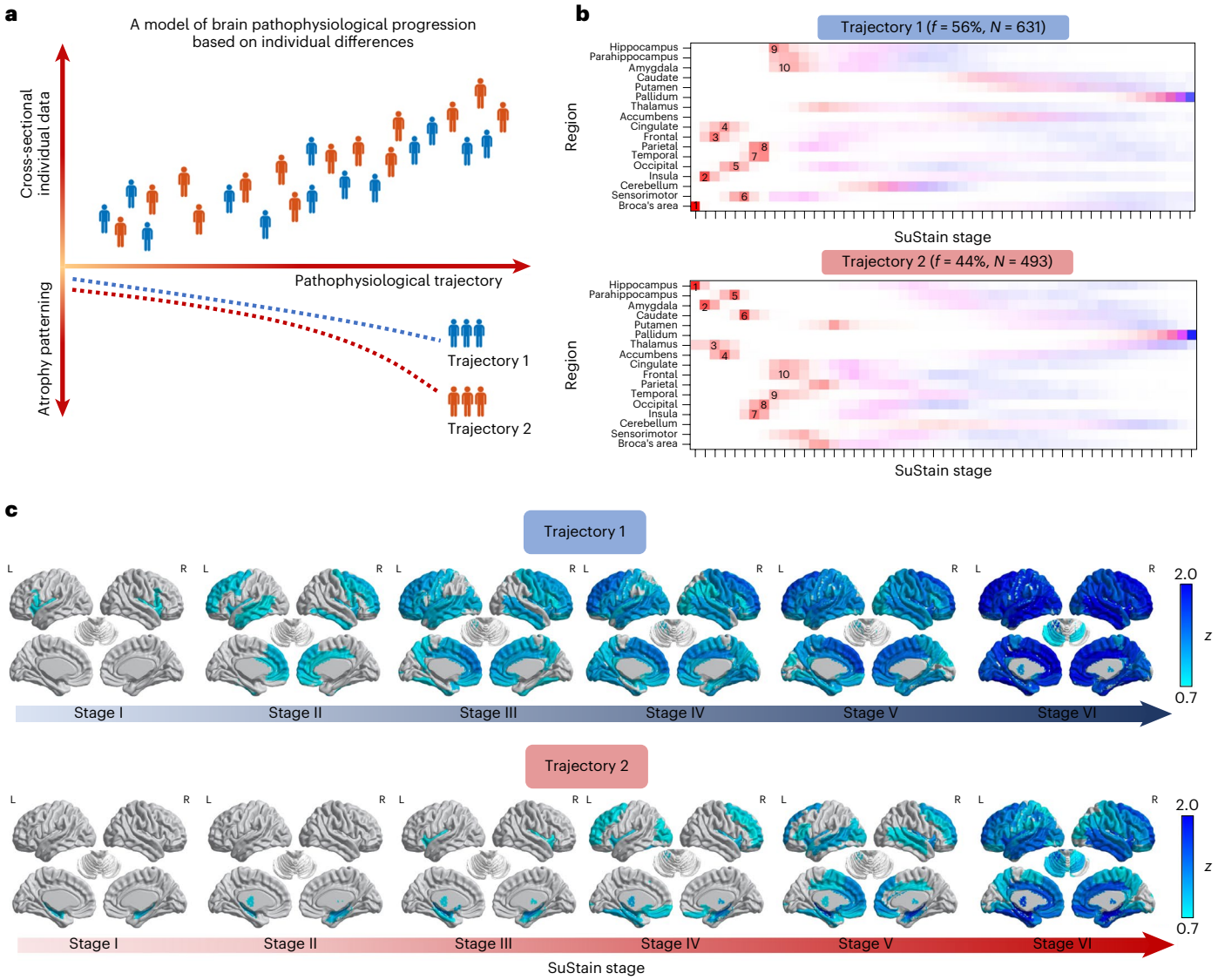

Fig. 1 | Pathophysiological progression of brain atrophy in schizophrenia. **a**, Data-driven disease-progression model (SuStaIn) was used to identify population subtypes with a common pattern of pathophysiological trajectory by disentangling phenotypic heterogeneity and temporal heterogeneity on cross-sectional individual data. **b**, Atrophy sequences of specific brain regions obtained using SuStaIn. The positional variance diagrams visualize the cumulative probability that each brain region has reached a particular *z* score using different colours. The colour indicates the level of severity of GMV loss: red is mildly affected (*z* score = 1, that is, 1 s.d. from healthy control average), magenta is moderately affected (*z* score = 2) and blue is severely affected (*z* score = 3). Colour density represents the proportion of the posterior distribution in which events (*y* axis) appear in a particular position in the sequence (*x* axis); *f* is the proportion of individuals assigned to each phenotype. Arabic numbers 1–10 marked against brain regions in the variance diagram indicate the order of the first ten events with brain-region atrophy, estimated by the SuStaIn. **c**, Pathophysiological trajectory. The mean *z* score images of GMV were derived across patients with schizophrenia belonging to stage bins (I, II, III, V, IV and VI) and mapped to a glass brain template for visualization using BrainNetViewer (https://www.nitrc.org/projects/bnv/). Regional volume loss at each stage bin shows a progressive spatial expansion pattern but differs between trajectories. In trajectory 1, volume loss is observed first in Broca's area and the insula (stage I), then in the anterior cingulate, prefrontal and lateral temporal cortices (stage II), then in the orbitofrontal and sensorimotor cortices (stage III), then in the occipital, parietal and temporal cortices (stages IV and V) and finally in the cerebellum and subcortical regions (stage VI). In trajectory 2, volume losses occur first in the hippocampus and amygdala (stage I) and then involve the parahippocampus, thalamus and accumbens (stage II), then the caudate and insula (stage III), followed by the putamen, cingulate, frontal and temporal lobes (stages IV and V) and finally the other cortical areas (stage VI). L, left; R, right.

general psychopathology were observed in subtype1, indicating a lower burden of non-negative symptoms in individuals with more atrophy. Interestingly, this pattern of relationship with non-negative symptoms was reversed in individuals within subtype2 (Extended Data Fig. 2 and Supplementary Tables 7 and 8), suggesting that associations between brain atrophy and symptoms are subtype-specific in schizophrenia.

Different clinical profiles among subtypes

We compared demographic, clinical and brain variables (Table 1) across the two stages and the two subtypes. The pre-atrophic patients with subcortical-primacy subtype2 ($S2_{pre}$) had shorter illness duration compared with all other individuals, including the $S1_{post}$ and $S2_{post}$ (Fig. 3a). The pre-atrophic patients with cortical-primacy subtype1 ($S1_{pre}$) had worse positive symptoms compared with all other individuals, including the $S1_{post}$ and $S2_{post}$ (Fig. 3b). Further, as expected, the $S1_{post}$ and $S2_{post}$ showed smaller total GMV and larger total cerebrospinal fluid (CSF) volume compared with $S1_{pre}$ and $S2_{pre}$ (Table 1). We also compared the differences between the subtype1 ($S1_{pre}$ and $S1_{post}$) and subtype2 ($S2_{pre}$ and $S2_{post}$) and found worse positive symptoms in subtype1 compared with subtype2 (Supplementary Table 9).

https://doi.org/10.1038/s44220-023-00024-0

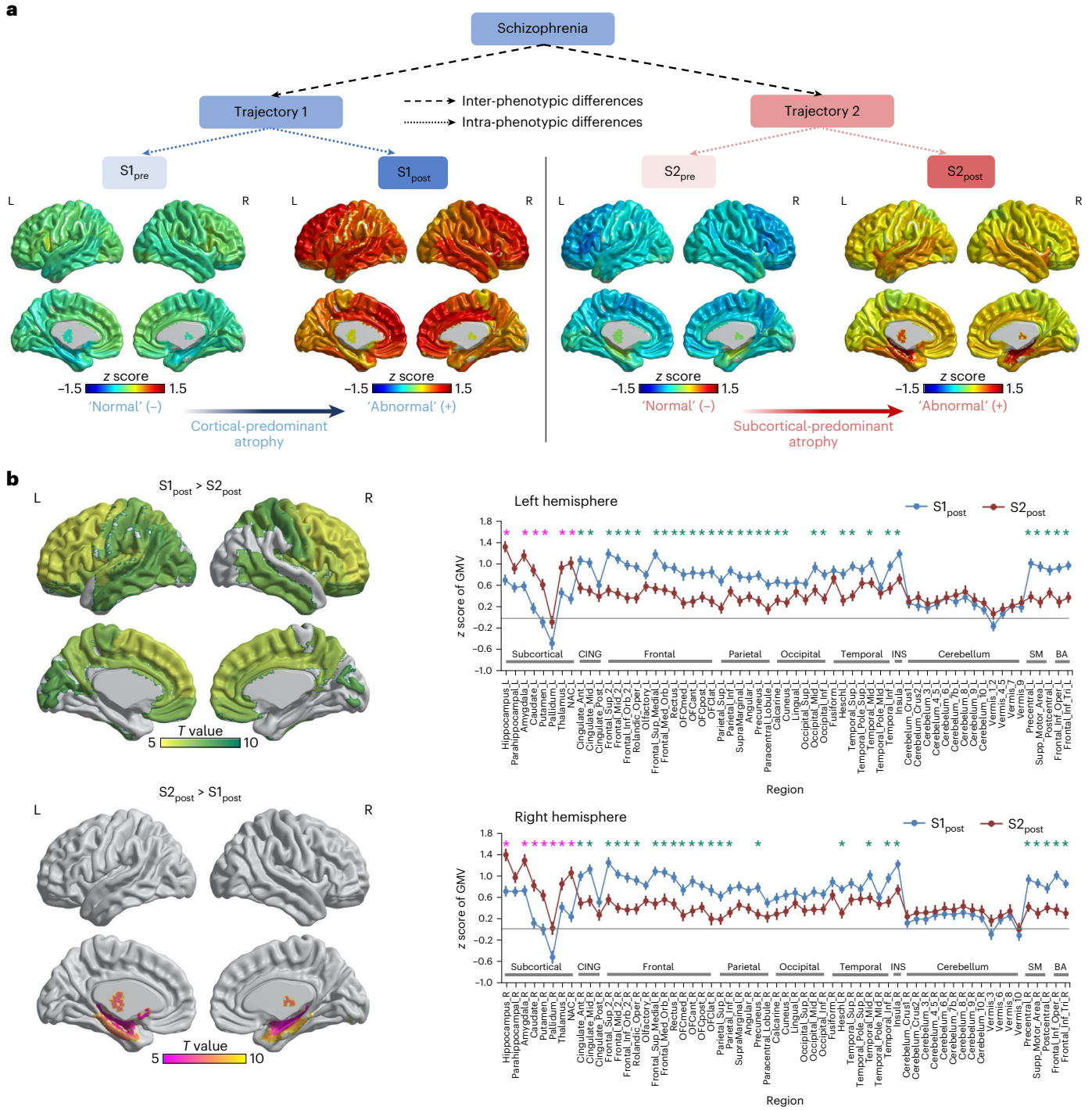

Fig. 2 | Atrophy patterns in four subtypes of schizophrenia. a, All individuals with schizophrenia were first classified into two phenotypes by distinct trajectories from SuStaIn on the basis of the inter-phenotypic differences (phenotypic heterogeneity). Individuals within each phenotype were further assigned into two subgroups according to which stage of the trajectory they belong to on the basis of the intra-phenotypic differences (temporal heterogeneity). By disentangling temporal heterogeneity and phenotypic heterogeneity, we identified four subtypes: trajectory 1 pre-atrophy ($S1_{pre}$, $n = 259$), trajectory 2 pre-atrophy ($S2_{pre}$, $n = 212$), trajectory 1 post-atrophy ($S1_{post}$, $n = 372$) and trajectory 2 post-atrophy ($S2_{post}$, $n = 281$). The atrophy pattern of whole grey matter (revealed by the mean z score of GMV) in four subgroups was mapped to a glass brain template for visualization. **b**, Comparison of the mean z score of GMV across all ROIs after adjusting for sex, age, the square of age, TIV and sites. The adjusted GMV values were normalized relative to the control population to derive z scores (a value of $z = 0$ represents the normal level in the control population). These z scores were multiplied by −1 so that the z scores would increase as the regional volumes decrease in patients with schizophrenia. Note that a higher z score (or T value) indicates a larger reduction of GMV; cortical GMV is more extensively reduced in $S1_{post}$ than in $S2_{post}$, but subcortical GMV reduction is more pronounced in $S2_{post}$ than in $S1_{post}$. Data are presented as mean values ± s.e.m. *Significant difference between the $S1_{post}$ ($n = 372$) and $S2_{post}$ ($n = 281$) using two-sample t test (two-sided $P < 0.001$, Bonferroni correction). Exact P values are provided in Supplementary Table 14. CING, cingulate cortex; INS, insula; SM, sensorimotor; BA, Broca's area.

https://doi.org/10.1038/s44220-023-00024-0

Table 1 | Comparison of variables between subtypes in the cross-sectional discovery sample

	Subtype1 (n=631)		Subtype2 (n=493)	
	$S1_{pre}$	$S1_{post}$	$S2_{pre}$	$S2_{post}$
Number	259	372	212	281
Age (yr)	31.1 (12.1)	31.8 (13.1)	30.0 (12.2)	31.1 (13.3)
Sex (female/male)	115/144	155/217	94/118	115/166
Ethnicity (Han Chinese/ Hispanic/not Han Chinese and not Hispanic/unknown)	187/8/38/26	251/20/69/32	163/8/33/8	213/8/43/17
Race (Black or African American/Asian/White/ other/unknown)	14/188/38/3/16	36/252/57/3/24	13/163/28/2/6	18/215/33/2/13
Illness duration (yr) (n=388)	9.1 (10.2)	12.2 (11.7)[c]	7.4 (10.5)*[b,d]	11.1 (11.7)[c]
PANSS scores (n=750)				
Positive scale	18.5 (6.8)*[b,d]	16.9 (7.0)[a]	17.2 (6.7)	16.1 (7.0)[a]
Negative scale	15.1 (7.4)	16.3 (7.7)	15.9 (7.8)	16.0 (8.1)
General scale	34.2 (11.1)*[b,d]	33.3 (10.4)[a]	33.8 (10.8)	32.7 (11.3)[c]
Total score	67.9 (22.0)*[d]	66.5 (20.80)	66.9 (21.0)	64.9 (22.1)[a]
TIV (cm^3)	1,500.8 (163.1)	1,498.6 (162.6)	1,500.1 (168.3)	1,488.4 (177.2)
Total GMV (cm^3)	674.2 (72.4)*[b,d]	635.3 (72.2)*[a,c]	687.3 (82.6)*[b,d]	643.8 (74.2)*[a,c]
Total WM volume (cm^3)	516.6 (59.6)*[d]	509.6 (65.6)	512.4 (59.5)[d]	500.7 (64.4)*[a,c]
Total CSF volume (cm^3)	308.0 (65.7)*[b,d]	354.2 (71.8)*[a,c]	299.3 (62.8)*[b,d]	343.6 (79.9)*[a,c]

Standard deviations are given in parentheses where relevant. P values are two sided and corrected by multiple comparisons. For PANSS scores, variables are statistically compared among four groups after controlling sex, age, age^2, site and illness stage. WM, white matter. *Corrected P<0.05 (versus all other subtypes). [a]Corrected P<0.05 (versus $S1_{pre}$). [b]Corrected P<0.05 (versus $S1_{post}$). [c]Corrected P<0.05 (versus $S2_{pre}$). [d]Corrected P<0.05 (versus $S2_{post}$).

We also found a relationship between SuStaIn stage scores and illness duration, symptoms, and GM and CSF volumes. As expected, increasing SuStaIn stage scores were positively associated with longer illness duration (r = 0.208, P < 0.001; Fig. 3c), higher burden of negative symptoms (r = 0.127, P = 0.008; Fig. 3d), larger CSF volume (r = 0.353, P < 0.001; Fig. 3e) and smaller GM volume (r = −0.250, P < 0.001; Fig. 3f).

In addition, we compared the differences of positive and negative symptoms among individuals belonging to different SuStaIn stages using the analysis of variance (ANOVA) and post hoc tests. In the cortical-primacy subtype, individuals belonging to the later stage VI (higher atrophy) showed a higher score of negative symptoms compared with individuals in stages I, II, III and pre-stage I (individuals without atrophy in any region) (corrected P < 0.05) (Fig. 3g). In subcortical-primacy subtype, individuals belonging to pre-stage I (no atrophy) showed a higher score of positive symptoms compared with individuals in stage I (corrected P < 0.05) (Fig. 3h).

Treatment outcomes and subtypes

We examined whether subtype classification relates to differential treatment response to APM and TMS using a longitudinal independent cohort. As for the APM sample, we found a significant positive correlation between the probability of belonging to subtype1 and PANSS positive score reduction ratio (r = 0.127, P = 0.014; Fig. 4a), indicating that individuals who have a higher probability of being assigned to subtype1 showed better treatment outcomes. This significant correlation remained consistent even when controlling the factors, including baseline PANSS scores, sites, education, sex, age, illness stage and chlorpromazine equivalents (CPZ) (Supplementary Table 11). As for the TMS follow-up sample, we observed a significant negative correlation between the SuStaIn stages and PANSS reduction ratio in terms of positive score (r = −0.370, P < 0.00001; Fig. 4b), general score (r = −0.237, P = 0.003) and total score (r = −0.279, P < 0.001), indicating that individuals with an earlier SuStaIn stage showed better treatment outcomes. The significant correlation between SuStaIn stage and symptom remission remained consistent when even controlling the factors, including baseline PANSS scores, sites, education, sex, age and illness stage (Supplementary Table 12), and was observed in both subtype1 (r = −0.351, P = 0.001) and subtype2 (r = −0.395, P < 0.001).

We also compared the differences of follow-up PANSS between subtype1 and subtype2. For individuals who were treated with APM, we found that compared with subtype2, subtype1 showed significant better positive symptoms remission after controlling the baseline PANSS (Fig. 4c and Supplementary Table 10). This difference remained consistent even after controlling the effects of CPZ and illness stage. However, for the individuals who were treated with TMS, we did not observe a significant difference in symptom reduction between two subtypes.

In addition to the two phenotypic subtypes, we compared the differences of follow-up PANSS among the four subgroups ($S1_{pre}$, $S1_{post}$, $S2_{pre}$ and $S2_{post}$). For APM, $S1_{pre}$ exhibited better treatment outcomes, especially with regard to the positive and general symptoms (Table 2 and Fig. 4d), compared with the other subgroups after controlling the baseline PANSS, CPZ and illness stage. For TMS, $S1_{pre}$ and $S2_{pre}$ showed more PANSS positive score reduction compared with $S1_{post}$ and $S2_{post}$ (Supplementary Table 13 and Fig. 4e), indicating better TMS outcome from treating positive symptoms for these individuals with less brain atrophy. These findings remained consistent even when controlling the factors of baseline PANSS, illness stages and TMS targets. We observed that in $S2_{pre}$, TMS exhibited better improvement in treating negative symptoms (Supplementary Table 13 and Fig. 4e).

All together, antipsychotics are more effective in the cortical-primacy type (subtype1) while superior outcomes with TMS are seen in pre-atrophic stages (for both $S1_{pre}$ and $S2_{pre}$). One specific case where TMS may be of benefit is the treatment of negative symptoms in the subcortical-primacy type before atrophy sets in ($S2_{pre}$). Once atrophy sets in, antipsychotics work better for reducing positive symptoms.

Discussion

Using a data-driven modelling technique, we show that pathological atrophy of schizophrenia is better characterized by two distinct pathophysiological trajectories: a cortical-predominant phenotype that

https://doi.org/10.1038/s44220-023-00024-0

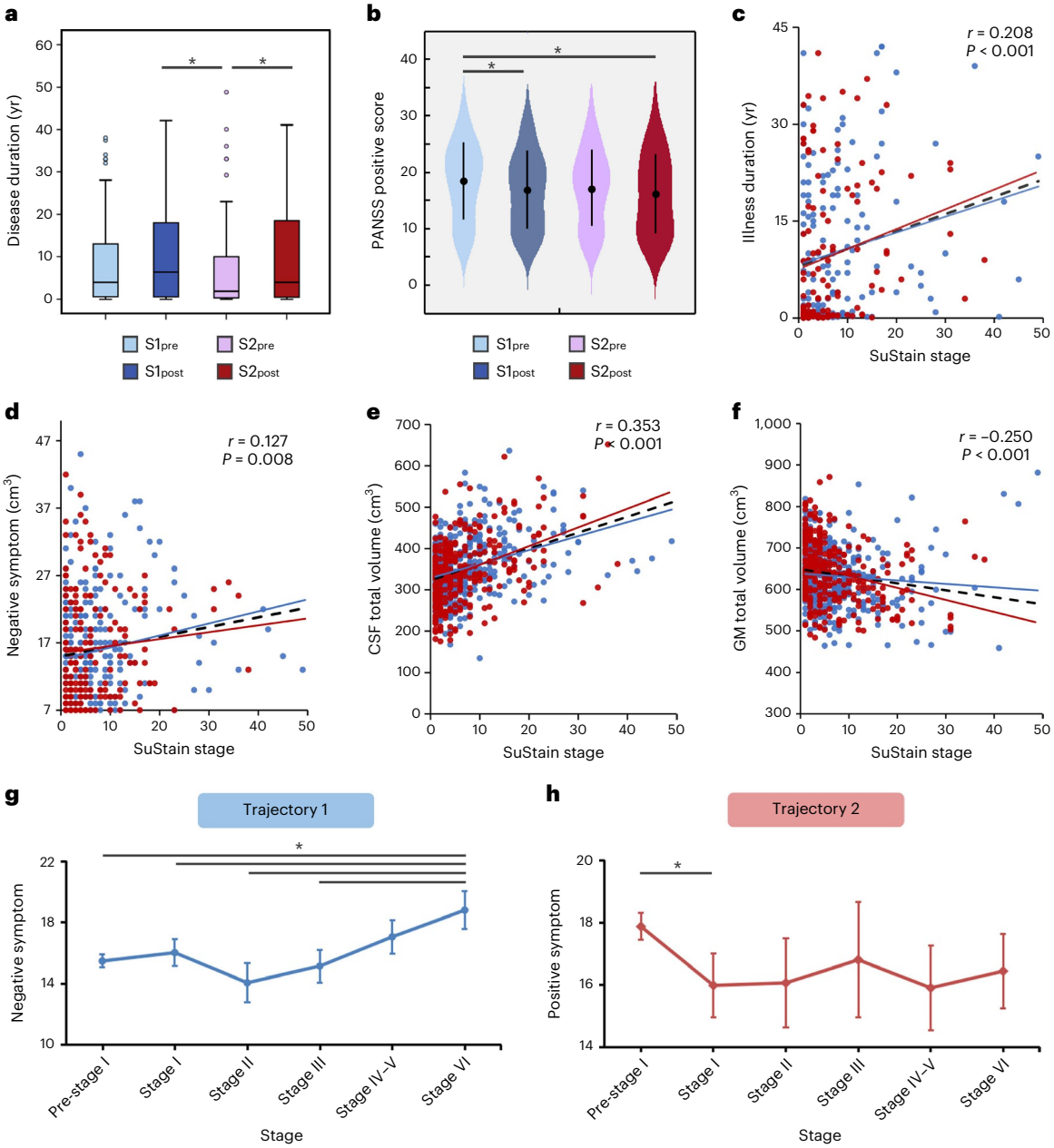

Fig. 3 | Subtypes characterized by clinical variables. a, Subtype differences of disease duration among the $S1_{pre}$ ($n = 77$), $S1_{post}$ ($n = 124$), $S2_{pre}$ ($n = 83$) and $S2_{post}$ ($n = 104$). Data are presented using a box plot (centre line, median; box limits, upper and lower quartiles; whiskers, 1.5 × interquartile range; points, outliers). **b**, Subtype differences of positive symptom burden among the $S1_{pre}$ ($n = 167$), $S1_{post}$ ($n = 242$), $S2_{pre}$ ($n = 153$) and $S2_{post}$ ($n = 188$). Data are presented as mean values ± s.d. **c**–**f**, Increasing SuStaIn stage was associated with longer illness duration ($r = 0.208$, $P = 4.6 \times 10^{-4}$) (**c**), worse negative symptoms ($r = 0.127$, $P = 0.008$) (**d**), larger CSF volume ($r = 0.353$, $P = 1.7 \times 10^{-22}$) (**e**) and less GMV ($r = -0.250$, $P = 1.1 \times <10^{-11}$) (**f**) across all subtypes, by false discovery rate correction. **g**, In trajectory 1 (pre-stage I, $n = 167$; stage I, $n = 71$, stage II, $n = 39$, stage III, $n = 37$, stage IV–V, $n = 46$, stage VI, $n = 49$), individuals belonging to stage VI showed a higher score of negative symptoms compared with individuals belonging to stage I, II, III and pre-stage I (individuals without obvious atrophy in any regions) (corrected $P < 0.05$). Data are presented as mean values ± s.e.m. **h**, In trajectory 2 (pre-stage I, $n = 153$; stage I, $n = 62$, stage II, $n = 39$, stage III, $n = 24$, stage IV–V, $n = 35$, stage VI, $n = 28$), individuals belonging to later stages (especially stage I; corrected $P < 0.05$) showed a lower score of positive symptoms compared with the stage before any atrophy is detectable. Data are presented as mean values ± s.e.m. The asterisks (*) in a,b,g,h indicate significant differences between the two subgroups using ANOVA with post hoc tests (two-sided $P < 0.05$, correction for multiple comparisons).

begins in the Broca's area/frontoinsular cortex and a subcortical-predominant phenotype that begins in the hippocampus. These subtypes showed different illness durations, symptom profiles and treatment outcomes. These findings raise critical research questions for stratified clinical trials in schizophrenia and indicate biological plausibility and therapeutic relevance of the identified subtypes.

Two distinct pathophysiological trajectories of brain atrophy were identified as cortical-predominant phenotype and subcortical-predominant phenotype. This indicates two possible sites of pathophysiological origin: cortical atrophy begins in the Broca's area and the frontoinsular cortex while subcortical atrophy begins at the hippocampus. Abnormalities in Broca's area have been found widely in schizophrenia[28]. Further, our previous studies found that individuals at high risk of psychosis exhibited functional connectivity changes primarily in the Broca's area[29], suggesting that dysfunction of Broca's area, possibly influenced by distinct genetic pathways[30],

https://doi.org/10.1038/s44220-023-00024-0

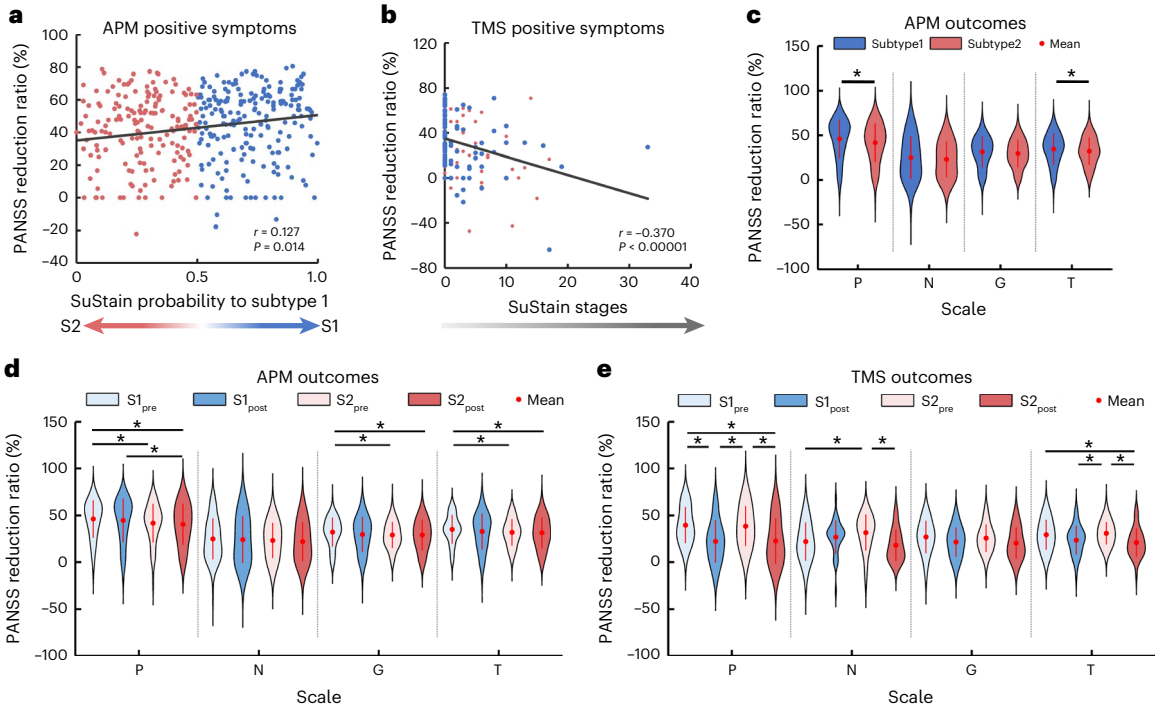

Fig. 4 | Treatment outcome and subtypes of schizophrenia in patients with follow-up data. a, The SuStaIn probability of belonging to subtype1 correlates significantly with the reduction ratio of PANSS positive symptoms scores when using APMs by Spearman correlation test ($r = 0.127$, $P = 0.014$, two sided). **b**, The progressive SuStaIn stages relate to a significantly lower PANSS positive symptoms reduction ratio when administering TMS by Spearman correlation test ($r = -0.370$, $P = 3.1 \times <10^{-6}$, two sided). **c**, Differences in APM-related PANSS reduction ratio across domains ($P = 0.003$ for PANSS positive scale; $P = 0.019$ for PANSS total score) between subtype1 ($n = 202$) and subtype2 ($n = 171$) in schizophrenia. **d**, Differences in APM-related PANSS reduction ratio among the $S1_{pre}$ ($n = 96$), $S1_{post}$ ($n = 106$), $S2_{pre}$ ($n = 70$) and $S2_{post}$ ($n = 101$). From left to right, the significant differences are marked by the asterisk (PANSS positive subscale: $P = 0.033$ for $S1_{pre} > S2_{pre}$, $P = 0.005$ for $S1_{pre} > S2_{post}$, $P = 0.037$ for $S1_{post} > S2_{post}$; PANSS general subscale: $P = 0.038$ for $S1_{pre} > S2_{pre}$, $P = 0.017$ for $S1_{pre} > S2_{post}$; PANSS total score: $P = 0.028$ for $S1_{pre} > S2_{pre}$, $P = 0.006$ for $S1_{pre} > S2_{post}$). **e**, Differences in TMS-related PANSS reduction ratio among the $S1_{pre}$ ($n = 47$), $S1_{post}$ ($n = 38$), $S2_{pre}$ ($n = 29$) and $S2_{post}$ ($n = 36$) for patients with schizophrenia receiving TMS. From left to right, the significant differences are marked by the asterisk (PANSS positive scale: $P = 0.0004$ for $S1_{pre} > S1_{post}$, $P = 0.0006$ for $S1_{pre} > S2_{post}$, $P = 0.004$ for $S2_{pre} > S1_{post}$, $P = 0.005$ for $S2_{pre} > S2_{post}$; PANSS negative scale: $P = 0.037$ for $S2_{pre} > S1_{pre}$; $P = 0.003$ for $S2_{pre} > S2_{post}$; PANSS total score: $P = 0.019$ for $S1_{pre} > S2_{post}$, $P = 0.037$ for $S2_{pre} > S1_{post}$, $P = 0.005$ for $S2_{pre} > S2_{post}$). Data in c,d,e are presented as mean values ± s.d. The asterisks (*) in c,d,e represent significant differences between the two subgroups using ANOVA with post hoc tests (two-sided $P < 0.05$, correction for multiple comparisons). P, PANSS positive subscale; N, PANSS negative subscale; G, PANSS general subscale; T, PANSS total score.

had emerged even before the first psychotic episode. Current results also provide direct structural imaging evidence that the Broca's area and adjacent frontoinsular cortex may be one of the 'sites of origin' of brain abnormalities in schizophrenia. These findings contribute to a key neuropathological role of Broca's area, in line with Crow's linguistic primacy hypothesis[31] and the frontoinsular-cingulate cortex, in line with the salience network model[32].

In subtype2, subcortical atrophy began at the hippocampus, another possible site of origin identified here. Some studies have highlighted hippocampal atrophy as one of the first regions to show volumetric loss in schizophrenia[8,33]. Recently, a longitudinal clinical high-risk psychosis study reported that for individuals who experience a prodromal stage to syndromal psychosis, hippocampal pathology (such as glutamate excess and hypermetabolism) leads to volume loss and expands to other regions of the hippocampal circuit and other connected areas along with illness progress[34]. Together, these findings challenge the notion that there is a single unifying pathophysiological process in schizophrenia, although this will require validation.

We note that as the degree of atrophy progresses with longer illness, individuals exhibited worse negative symptoms irrespective of their subtypes. Interestingly, both the cortical- and subcortical-primacy subtypes showed worse positive symptoms when atrophy was limited (positive symptom correlation in subtype1 (Extended Data Fig. 2); pre-stage I versus stage I comparison for subtype2 (Fig. 3h)). While this may appear counterintuitive at the outset, this lends support to the emerging notion that the progressive grey-matter changes in schizophrenia may indeed be a feature of cortico-subcortical reorganization in response to positive symptoms[10,14]. Thus, unlike a degenerative process in which tissue reduction will predict worse clinical symptoms, such reduction in schizophrenia may alleviate the positive symptoms, at the cost of worsening negative symptoms[35]. This notion may also contribute to understanding why, in general, antipsychotic exposure hastens brain tissue loss in schizophrenia[14,36], although it is still a complex and fiercely debated topic. We also found that patients with longer illness duration had lower positive subscale and higher negative subscale. It was consistent with a previous longitudinal work[37], revealing that the positive symptoms exhibited a general pattern of improvement while negative symptoms showed less reduction over time. We also noticed the inconsistency of inter-subtype symptom difference between the cross-sectional and longitudinal samples, which may be due to the heterogeneity of psychotic symptoms and stages of illness[38,39].

The combined subtyping and staging approach employed here also highlights the prognostic potential of MRI. By MRI subtyping, we found 'what kind of brain' and 'at which stage' is more likely to benefit from specific treatments, providing preliminary support for the prognostic potential of schizophrenia biotypes. Our data revealed that antipsychotics outcome is related to phenotypic subtype while TMS is associated with stage subtype. These results are consistent with studies reporting that schizophrenia patients with specific brain features may benefit from specific interventions. For example, volume increase in the hippocampus predicted negative symptom

https://doi.org/10.1038/s44220-023-00024-0

Table 2 | Comparisons of treatment outcomes among four SuStaIn subgroups in a longitudinal sample of 373 patients with schizophrenia treated with APMs

	Subtype1 (*n*=202)		Subtype2 (*n*=171)	
	$S1_{pre}$	$S1_{post}$	$S2_{pre}$	$S2_{post}$
Number	96	106	70	101
Age (yr)	25.0 (7.5)[d]	26.4 (9.0)	25.1 (7.7)[d]	28.5 (10.6)[a,c]
Sex (female/male)	49/47	54/52	36/34	51/50
Education (yr)	12.9 (2.7)	13.2 (2.8)	12.6 (2.7)	12.8 (3.0)
Illness duration (yr)	2.8 (4.7)[d]	4.7 (7.3)	3.3 (5.1)	5.2 (8.3)[a]
CPZ ($mg\,d^{-1}$)	384.8 (219.3)	383.9 (200.6)	368.9 (229.7)	375.3 (207.1)
Responders (%)	79.17	66.98	71.43	69.31
Baseline PANSS				
Positive subscale	22.5 (5.1)	22.4 (7.0)	23.3 (4.7)	22.6 (6.4)
Negative subscale	17.9 (6.1)*[c,d]	19.4 (7.4)	20.1 (6.5)[a]	21.1 (6.9)*[a]
General subscale	38.2 (6.8)	38.8 (8.6)	39.9 (7.2)	40.2 (8.4)
Total score	78.6 (12.9)*[c,d]	80.5 (18.3)	83.3 (12.7)[a]	84.2 (15.5)*[a]
Follow-up PANSS				
Positive subscale	11.6 (4.6)	11.3 (4.7)[c]	13.1 (4.5)*[b]	12.5 (4.5)
Negative subscale	13.2 (5.4)*[c,d]	14.8 (8.4)	15.0 (5.2)[a]	16.3 (6.4)*[a]
General subscale	25.3 (6.0)*[c,d]	26.3 (6.6)	27.8 (6.4)[a]	27.6 (5.9)[a]
Total score	50.1 (13.3)*[c,d]	52.1 (14.5)[d]	56.0 (13.5)[a]	56.2 (13.6)*[a,b]
PANSS reduction ratio (%)				
Positive subscale	46.7 (20.1)*[c,d]	45.2 (23.4)[d]	42.3 (20.7)[a]	41.1 (22.1)*[a,b]
Negative subscale	22.1 (30.8)	15.5 (46.1)	23.1 (20.3)	19.9 (28.5)
General subscale	32.7 (15.6)*[c,d]	29.6 (20.3)	29.6 (14.0)[a]	29.5 (16.4)[a]
Total score	35.6 (15.5)*[c,d]	32.9 (20.5)	32.4 (14.2)[a]	31.9 (16.5)[a]

Standard deviations are given in parentheses where relevant. *P* values are two sided and corrected by multiple comparisons. At follow-up, patients whose symptom burden, measured as percentage reduction ratio in PANSS total score, dropped >25% were defined as responders. *Corrected P < 0.05 (versus all other subtypes). [a]Corrected *P* < 0.05 (versus $S1_{pre}$). [b]Corrected *P* < 0.05 (versus $S1_{post}$). [c]Corrected *P* < 0.05 (versus $S2_{pre}$). [d]Corrected *P* < 0.05 (versus $S2_{post}$).

improvement for TMS[40]. Our study observed that patients who better respond to APM had stronger cortico–cortical connectivity compared with non-responders[14]. It should be noted, however, that medication use of the current sample is highly heterogeneous, involving monotherapy and combined therapy and including up to ten antipsychotic drugs. Although identifying potential mechanisms is still challenging, the subtypes we report parse the heterogeneity of the brain features and map them to specific treatments. These results suggest that prediction of treatment outcome may benefit from stratification based on biological subtypes of schizophrenia.

This study has several limitations. First, the SuStaIn creates pseudo-longitudinal sequences using cross-sectional data. The fitted pathophysiological trajectories do not directly reflect the real illness progression. Although longitudinal data support the truth of SuStaIn trajectories (mainly the early stage of the trajectory), future work needs to verify the pathophysiological trajectories. Not all individuals with schizophrenia had quantitative medication information, which limited our ability to eliminate the medication impact. Second, it is unclear whether MRI-based estimates reflect true tissue atrophy. In addition to GMV, cortical thickness or gyrification could also be considered. The current mixed sample had confounding factors from different cohorts, scanners and sites. Harmonization methods[41] should be used to alleviate differences across MRI acquisition protocols. Patients undergoing TMS also received APM. Ideally, randomizing individuals with comparable illness duration to APM or TMS, and reducing variations in medication choice and the site of TMS stimulation, would have improved the out-of-sample generalizability of our findings. Robust demonstration of clinical utility of the subtypes requires prospective trials in the future. Finally, while clustering/subgrouping may aid in stratified interventions, considerable variability may still exist among individuals within a cluster; dimensional approaches to personalization may be more appropriate to address this issue[42]. We have not tested the extent to which the subtypes identified here could account for the heterogeneity; a continuous representation of neurobiological changes may be superior in this regard, but this needs to be tested.

In conclusion, we describe two distinct but stable pathophysiological trajectories of brain atrophy of schizophrenia, separately beginning in Broca's area and the hippocampus. These subtypes exhibit different atrophy patterns, clinical symptom profiles and treatment outcomes. Antipsychotics are more effective in the cortical-primacy type while superior outcomes with TMS are seen in the pre-atrophic stage of illness irrespective of the phenotypic subtype. These findings suggest that distinct pathophysiological processes underlie schizophrenia and that they potentially yield to stratification and prognostication, which are key requirements for personalizing treatments in enduring illnesses.

Methods

Sample characteristics

Cross-sectional sample. The primary sample consisted of cross-sectional T1-weighted MRI scans from 2,239 individuals (1,168 patients with schizophrenia) from 4 hospitals—Shanghai Mental Health Centre (dataset #1), First Affiliated Hospital of Zhengzhou University (dataset #2), Taipei Veteran General Hospital (dataset #3) and Clinical Hospital of Chengdu Brain Science Institute in Chengdu (dataset #4)—and from

another 5 publicly available datasets: COBRE (dataset #5), NMorphCH (dataset #6), FBIRN (dataset #7), NUSDAST (dataset #8) and DS000115 (dataset #9). All individuals with schizophrenia were diagnosed according to the *Diagnostic and Statistical Manual of Mental Disorders*, fourth edition (DSM-IV). Individuals were excluded from the study if they (1) were diagnosed with schizoaffective disorder, mood disorders or other major medical or neurologic disorders; (2) had alcohol/drug dependence; (3) had a history of electroconvulsive therapy within six months; (4) had other contraindications to MRI scanning. Individuals with illness duration less than two years were defined as FES. The data quality-control steps are described in Supplementary Method 4. After data quality control, 2,170 individuals were included, of which 1,124 were patients with schizophrenia (479 women, age = 31.1 ± 12.8 yr) and 1,046 were healthy participants (498 women, age = 32.6 ± 12.4 yr). Symptom severity was assessed with the PANSS for individuals from datasets #1, #2, #3, #4 and #5, with the Brief Psychiatric Rating Scale for individuals from dataset #8, and with the Scale for the Assessment of Positive Symptoms and Scale for the Assessment of Negative Symptoms for individuals from datasets #6, #8 and #9. Detailed information of each cohort is provided in Supplementary Method 1. A summary of demographics of subjects is given in Supplementary Table 1.

Longitudinal sample. A total of 373 patients with schizophrenia (190 women, age = 26.4 ± 9.0 yr) from four hospitals (Shanghai Mental Health Center (Shanghai), $N = 180$; Peking University People's Hospital (Beijing1), $N = 102$; Peking University Sixth Hospital (Beijing2), $N = 65$; Clinical Hospital of Chengdu Brain Science Institute (Chengdu), $N = 26$) were treated with APM and included in the longitudinal analyses (Supplementary Table 2). All individuals met DSM-IV diagnostic criteria for schizophrenia and no comorbid Axis I disorders. Inclusion and exclusion criteria of subjects are provided in our previous study[14]. At baseline, 294 participants were treatment-naïve FES. Following baseline MRI, 373 patients with schizophrenia received APM. Of these, 300 received monotherapy: amisulpride ($n = 26$), aripiprazole ($n = 58$), blonanserin ($n = 3$), clozapine ($n = 7$), olanzapine ($n = 85$), paliperidone ($n = 15$), paliperidone palmitate injection ($n = 4$), quetiapine ($n = 8$), risperidone ($n = 87$), ziprasidone ($n = 3$) and unknown ($n = 4$). The remaining 73 patients received combined therapy (≥two antipsychotic drugs). The daily dosage of drugs was converted to CPZ. The mean CPZ during medication was 378.9 ± 210.0 mg d^{-1}. The severity of symptoms was evaluated on the basis of PANSS administered by the same psychiatrist. Symptom relief indicated in PANSS total and subscale scores (reduction ratio = (baseline − follow-up)/baseline × 100%) was used to measure treatment response. The average duration of PANSS follow-up was 9.6 weeks. At follow-up, 267 of 373 (71.6%) patients with schizophrenia were considered as APM responders, whose symptom relief (percentage of reduction ratio in PANSS total score) was >25%. Information on antipsychotic medication usage is provided in Supplementary Table 3.

A total of 150 patients with schizophrenia (66 women, age: = 30.1 ± 12.3 yr) from four hospitals (First Affiliated Hospital of Anhui Medical University (Anhui), $N = 38$; Fourth Military Medical University (Xi'an), $N = 36$; Clinical Hospital of Chengdu Brain Science Institute (Chengdu), $N = 27$; Harbin First Specialized Hospital (Harbin), $N = 49$) were treated with TMS under stable dosage of antipsychotics and included in the longitudinal analyses. At baseline, 100 of them were treatment-naïve FES. The inclusion criteria and TMS parameters are detailed in Supplementary Method 3. In brief, the stimulation target was set at the left temporoparietal junction for 74 individuals, at the left dorsolateral prefrontal cortex for 27 individuals and at the right orbitofrontal cortex for 49 individuals. PANSS assessments were performed at baseline and at follow-up by the same psychiatrist. The average duration of PANSS follow-up was 4.0 weeks. At follow-up, 82 of 150 (54.7%) patients with schizophrenia were considered as TMS responders, whose percentage of reduction ratio in PANSS total score was >25%. A summary of demographics of participants who were treated by APM or TMS is provided in Supplementary Table 2. We use the naturalistic data from APM and TMS samples collected during routine clinical care; this is not a report of a randomized trial. The TMS study was registered in the Chinese Clinical Trials Registry (number ChiCTR2000041106) and the TMS protocol was available (http://www.chictr.org.cn/showproj.aspx?proj=65566). Written informed consent was obtained from all participants and/or their legal guardians. Participants received travel compensation and remuneration up to 300 Chinese Yuan depending on the study they participated in.

Ethics and inclusion statement. The study included local researchers throughout the research process—study design, study implementation, data ownership, intellectual property and authorship of publications. The relevant roles and responsibilities were agreed among collaborators ahead of the research. The study has been approved by the Medical Research Ethics Committees of the local hospitals (ethics numbers 2017-36R (dataset#1), 2018-KY-88 (dataset#2), YM105091F (dataset#3), CDFH2014030501 (dataset#4), 2017-36R (Shanghai), 2008-2 (Beijing1), 2017-16 (Beijing2), CDFH2014030501 (Chengdu), 2016003 (Anhui), XJYYLL-2015047 (Xi'an) and IRB2019-004 (Harbin)).

Image acquisition and processing

The T1-weighted MRI acquisition procedures (including the longitudinal sample) for each cohort have been described previously[12,14,43,44]. The T1-weighted images were processed using the Computational Anatomy Toolbox (http://www.neuro.uni-jena.de/cat/) within SPM12 (https://www.fil.ion.ucl.ac.uk/spm/software/spm12/). Briefly, a fully automated procedure for standard voxel-based morphometry (including spatial registration, tissue segmentation and bias correction of intensity non-uniformities) was conducted, resulting in GMV images. The GMV images were parcellated on the basis of the automated anatomical (AAL) atlas. These parcellations were used to extract mean GMV values within different ROIs for each subject.

SuStaIn

Traditional data-driven subtyping of brain imaging in schizophrenia has low replicability due to the confounding effect of illness stage. Most clustering methods classify individuals on the basis of their symptoms, cognitive scores or structural or functional neuroimaging features. All of these features change with disease progression; thus, the assumption that all individuals are at the same stage of illness when measurements are obtained is fallacious. Here we model disease progression in schizophrenia as a linear deviation from normality of brain structure (see Supplementary Method 5 for further discussion on this assumption). A new approach, SuStaIn generates clustering solutions across participants while accounting for disease progression[26] (Fig. 1a). SuStaIn has demonstrated the ability to identify diverse but distinct progression patterns using cross-sectional neuroimaging data for brain disorders[26,27].

The SuStaIn approach has been presented in detail in a previous publication[26]; we briefly describe the major features here. The *z* score model underlying SuStaIn is a development of the original event-based model[45]. The event-based model regards disease progression as a series of events, where each event corresponds to a switch from a normal to an abnormal level for a biomarker/feature[45]. The linear *z* score SuStaIn model reformulates the events that represent the continuous linear accumulation (more biologically plausible) of a biomarker/feature from one *z* score to another rather than a discrete event-related transition towards an abnormal state[26]. See Supplementary Method 5 for a discussion on the validity of this assumption in schizophrenia.

***z* scores.** The data for SuStaIn need to be *z* scored relative to a control population. The *z* scores represent the severity of an abnormality for a specific feature/biomarker of interest, in this case, MRI-derived GMV. Higher *z* scores represent larger deviations from the normal (more

severe atrophy, in this case). In this study, the ROI-wise GMV values were first adjusted by regressing out the effects of sex, age, age^2, total intracranial volume (TIV) and sites as dummy covariates using a regression model. We did not include ethnicity in the regression model due to similar covarying tendencies of ethnicity and site (dataset#1–dataset#4 for Han Chinese; dataset#5–dataset#9 for not Han Chinese). Subsequently, the adjusted GMV values were normalized relative to the control population using *z* scores. Finally, these *z* scores representing normative deviations were multiplied by −1 so that as the regional brain volumes decrease in patients with schizophrenia, the *z* scores increase.

Input features. Input for SuStaIn requires an $M \times N$ *z* score matrix, where M represents the number of patients with schizophrenia ($M = 1{,}124$ in this study) and N represents the number of SuStaIn features/ROIs ($N = 17$ here). In this case, SuStaIn features represent the mean *z* scores of GMV within different ROIs. Due to computational complexity (Supplementary Method 6) and sufficient power of sample size, SuStaIn models typically used approximately 15 ROIs in previous studies[26,27]. Here, all of the AAL ROIs of whole brain were separated into 17 features (frontal lobe, temporal lobe, parietal lobe, occipital lobe, insula, cingulate, sensorimotor, Broca's area, cerebellum, hippocampus, parahippocampus, amygdala, caudate, putamen, pallidum, nucleus accumbens and thalamus) (Supplementary Fig. 1a). See Supplementary Table 4 for a summary of the features used in the SuStaIn modelling. On the basis of previous literature[26], we used *z* scores = 1 (1 s.d. from normal), 2 and 3 as severity cut-offs indicating waypoints of disease progression for the included features.

Sequence estimation. We imported 17 ROIs, each ROI having 3 severity cut-offs (z = 1, 2, 3), to the model of SuStaIn, yielding a total of 51 events to be sequenced. The most probable sequence ($S_k = (e_1, e_2, \ldots, e_{51})$) of spatial progression (trajectory) for each subtype was then evaluated using SuStaIn (see details in ref. [26]). SuStaIn assumes a uniform prior that all combinations of subtype and stage are equally probable. The model is initialized with an expectation–maximization algorithm and repeated for 25 different random start points to find the maximum likelihood solution. The number of all possible sequences is too large, so we evaluated the relative probability (uncertainty) of all possible sequences for each subtype using a 10,000 Markov chain Monte Carlo (MCMC) sampling (see details in ref. [26]). The cumulative probability for each feature/ROI to reach a particular *z* score over time is presented in Fig. 1b.

Number of subtypes. To establish the clustering tendency within the data, we employed Hopkins statistics[46], which provided a robust support for the existence of clusters (H = 0.8026, indicating a high clustering tendency at the 90% confidence level). SuStaIn could identify the potential distinct trajectories of pathophysiological progression with a given subtype number k. Previous clustering studies without progression-based modelling have reported two to six morphological subtypes of schizophrenia[19,47,48]. We used this range to estimate SuStaIn models separately. To determine the optimal number of subtypes with distinct trajectories, we measured the reproducibility of SuStaIn subtype by a twofold cross-validation method. Specifically, the cohort was randomly split into two non-overlapping subfolds (50% of the patients as one subfold and 50% as the other subfold). This procedure was repeated ten times to avoid the occasionality of one split. For each non-overlapping subfold, the SuStaIn model was trained on one of the non-overlapping folds, separately for each $k = 1$–6 subtypes, and further tested using the other non-overlapping subfold. The optimal subtype number was determined using three metrics. (1) Consistency of individual subtype assignment (Supplementary Fig. 3). For each individual, the subtype label was estimated separately in two non-overlapping subfolds. As the classification label may change for independent SuStaIn modelling (for example, Label 1 of train set may correspond to Label 6 of test set), the subtype label vector was transformed to an adjacent matrix. Dice coefficient was used to measure the consistency of the adjacent matrix between two non-overlapping subfolds. (2) Consistency of the SuStaIn trajectory (Supplementary Fig. 4). In each non-overlapping subfold, SuStaIn estimated the trajectory (the most probable sequence (S_k) of regions) for each subtype. The mean Kendall's tau coefficient between the S_k from paired subfolds was used to quantify the consistency in the SuStaIn trajectory. (3) Silhouette clustering evaluation criterion (Supplementary Fig. 5). In each non-overlapping subfold, Silhouette value was used as another evaluation indicator for subtype number range from 2 to 6. Supplementary Figs. 3–5 show that the optimal subtype number $k = 2$ is consistent by cross-validation, indicating the best fit to the data included two subtypes with two distinct pathophysiological progressions of GMV changes in schizophrenia. The two-cluster model of SuStaIn was fitted to the whole sample.

Visualization of distinct trajectories of grey-matter atrophy. To visualize the pathophysiological progression of grey-matter atrophy across SuStaIn stages, we calculated the mean *z* score images for individuals belonging to the following stage bins: I (e_1, e_2), II (e_3, e_4), III (e_5, e_6) and IV (e_7, e_8) for both subtypes; V(e_9, e_{10}) and VI (e_{11} to e_{51}) for subtype1; and V (e_9 to e_{12}) and VI (e_{13} to e_{51}) for subtype2. Regions with mean *z* score > 0.7 for regional volume loss are displayed. Two distinct trajectories of grey-matter atrophy are displayed in Fig. 1c.

Subtyping and staging at the individual level. For each individual with schizophrenia, SuStaIn calculated the likelihood of belonging to a subtype and a stage on the basis of the average position over the posterior distribution on the sequence via 10,000 Markov chain Monte Carlo iterations. Individuals were assigned to their maximum likelihood subtype first, and then the stage with the highest likelihood was determined. The proportion in each subtype and stage is provided as Supplementary Fig. 1b. Note that SuStaIn assigned individuals who do not display deviant GMV in any feature/ROI (here, z scores of all features are <1) into 'stage 0', which was defined as a pre-atrophy stage. As the SuStaIn classifies all individuals into clusters according to distinct sequences of GMV reductions in different brain regions, rather than clustering the individuals on the basis of their current atrophy degree, SuStaIn can categorize these individuals with similar atrophy sequences, even if the brain of some of these individuals has not atrophied to a notable degree (defined as $z = 1$ in this study). Supplementary Fig. 6 provides an example showing how pre-atrophy and post-atrophy individuals could be classified into the same subtype.

Subtype characterization

Subtype-specific atrophy patterns. To visualize atrophy patterns of whole grey matter for each subtype, we calculated the mean *z* score of GMV for each AAL atlas ROI. We compared the ROI-wise *z* scores between subtypes using independent samples *t* test (two sided). Multiple comparisons were corrected by Bonferroni correction $P < 0.001$. The ROI-wise *z* score images were further mapped to a glass brain template for visualization using BrainNetViewer (https://www.nitrc.org/projects/bnv/).

Association between regional atrophy and clinical symptoms. Within each subtype, we examined the relationships between regional atrophy and symptoms by deriving the Spearman coefficient between PANSS (positive, negative and general psychopathology subscales) and mean *z* score of GMV for each ROI, after adjusting for sex, age, age^2, TIV and sites. To correct for multiple comparisons, a permutation-based procedure was applied to control the family-wise error rate[49].

Distinct clinical profiles between subtypes. Demographic, clinical and global brain variables available for our discovery cohort included age ($n = 1{,}124$), sex ($n = 1{,}124$), illness duration ($n = 388$), PANSS ($n = 750$),

TIV (n = 1,124), total GMV (n = 1,124), total white-matter volume (n = 1,124) and total CSF volume (n = 1,124). To determine subtype-specific characteristics, these variables were statistically compared between subtype1 and subtype2 by using a regress model with sex, age, age^2, site and SuStaIn stage as covariates. Furthermore, individuals within each subtype were further divided into two subgroups (pre-atrophy and post-atrophy) on the basis of the degree of atrophy. Thus, the statistical comparison among the four subgroups ($S1_{pre}$, $S1_{post}$, $S2_{pre}$ and $S2_{post}$) involved two steps: (1) comparison with all other subgroups (one-versus-all comparison; a one-versus-all approach was used to compare each subgroup with all individuals of the other three subgroups to determine the subgroup-specific characteristics), and (2) comparison directly with each other subgroup (one-versus-one comparison) to assess the differences between subgroups. After testing for assumptions of normality and equal variances using the Kolmogorov–Smirnov test, quantile–quantile plot and Levene test (Supplementary Method 10), the statistical comparisons were conducted using ANOVA with appropriate post hoc tests (two sided), with false discovery rate (FDR) correction for the number of variables assessed.

We also investigated the relationship between the staging scores from SuStaIn and age, illness duration, symptoms, total GMV and total CSF volume using Spearman's correlation across the whole sample and stratified by subtype. Two-sided P values were FDR-corrected for the number of variables assessed.

Treatment outcomes across subtypes

In this exploratory analysis, we examined whether subtype classification based on baseline brain features will relate to differential treatment response to APM and TMS. A total of 373 patients with schizophrenia treated by APM and 150 patients with schizophrenia treated by TMS were included in the longitudinal analyses (Supplementary Table 2).

On the basis of the baseline MRI data, the SuStaIn model first assigned each individual with schizophrenia to one of two subtypes (phenotypic subtype1 or subtype2) according to the probability of belonging to which trajectory. Then individuals within each phenotype were further assigned to one of the stages on the basis of the SuStaIn trajectory. The SuStaIn probability score of subtype1 membership and the estimated SuStaIn stages were used as two quantitative indicators to measure their association with follow-up treatment outcomes. Following baseline MRI, individuals with schizophrenia received APM or TMS (details in the Supplementary Method 3). At follow-up, treatment outcome was measured by the reduction ratio (reduction ratio = (baseline − follow-up)/baseline × 100%) for PANSS total and subscale scores. Spearman correlation analysis between the preceding SuStaIn quantitative indicators and treatment outcomes was performed after controlling the baseline PANSS. We also compared the differences of follow-up treatment outcomes between the two phenotypic subtypes (subtype1 and subtype2) using the one-versus-all and one-versus-one statistical comparisons. In addition to the two phenotypic subtypes, we further classified individuals within each phenotype into two subgroups (pre-atrophy and post-atrophy) on the basis of the intra-phenotypic differences (temporal subtype). By disentangling both temporal heterogeneity and phenotypic heterogeneity, we further obtained four subgroups ($S1_{pre}$, $S1_{post}$, $S2_{pre}$ and $S2_{post}$). After testing for assumptions of normality and equal variances using the Kolmogorov–Smirnov test, quantile–quantile plot and Levene test (Supplementary Method 10), we compared the differences of follow-up treatment outcomes among the four subgroups using ANOVA with appropriate post hoc tests (two sided). A permutation-based family-wise error procedure was employed for controlling for multiple comparisons[49].

Replication analysis

To establish the SuStaIn validity for an alternative atlas, another three commonly used atlases (BN246 atlas, Schaefer200 atlas and HCP-MMP360 atlas) were applied for ROI extraction and SuStaIn modelling. To evaluate the stability of SuStaIn at a relative higher spatial resolution, the 17 AAL features were expanded to 22 and 27 features (AAL22 and AAL27) by a data-driven hierarchical clustering procedure. A total of five validation sets of features were generated to further verify the stability of SuStaIn (Supplementary Method 6). In addition, we examined the stability of SuStaIn trajectories using leave-one-site-out resampling (Supplementary Fig. 10). Finally, we performed post hoc power analyses for the primary results of this study using G*Power (https://www.psychologie.hhu.de/arbeitsgruppen/allgemeine-psychologie-und-arbeitspsychologie/gpower) (Supplementary Method 9).

Reporting summary

Further information on research design is available in the Nature Portfolio Reporting Summary linked to this article.

Data availability

Data of COBRE, NMorphCH, FBIRN and NUSDAST were obtained from the SchizConnect, a publicly available website (http://www.schizconnect.org/documentation#by_project). The NMorphCH dataset and NUSDAST dataset were download through a query interface at the SchizConnect (http://www.schizconnect.org/queries/new). The COBRE dataset was download from the Center for Biomedical Research Excellence in Brain Function and Mental Illness (COBRE) (https://coins.trendscenter.org/). The FBIRN dataset was download from https://www.nitrc.org/projects/fbirn/. The DS000115 dataset was download from OpenfMRI database (https://www.openfmri.org/). Data from the other datasets (cross-sectional datasets #1, #2, #3, #4, longitudinal AMP and TMS data) are not publicly available for download, but access requests can be made to the respective study investigators: cross-sectional data (datasets #1, #2, #3, #4)—corresponding author J. Feng; APM data—J. Wang (jijunwang27@163.com), X. Yu (yuxin@bjmu.edu.cn), W. Yue (dryue@bjmu.edu.cn) and C. Luo (chengluo@uestc.edu.cn); TMS data—J. Wang (jijunwang27@163.com), G. Ji (jigongjun@163.com), L. Cui (cui_fmmu@163.com) and C. Luo (chengluo@uestc.edu.cn). Requests for raw and analysed data can be made to the corresponding author J. Feng and will be promptly reviewed by the Fudan University Ethics Committee to verify whether the request is subject to any intellectual property or confidentiality obligations.

Code availability

Python of the SuStaIn algorithm is available on the UCL-POND GitHub (https://github.com/ucl-pond). The T1-weighted images were processed using the Computational Anatomy Toolbox (http://www.neuro.uni-jena.de/cat/) within SPM12 (https://www.fil.ion.ucl.ac.uk/spm/software/spm12/). The visualization of ROI-wise z score images was conducted using BrainNetViewer (https://www.nitrc.org/projects/bnv/). Statistical analyses, including correlation analysis, t test and ANOVA, were conducted using MATLAB (version: R2018b) and SPSS Statistics (version: 26.0). Other custom codes developed in the current study are available at GitHub (https://github.com/YuchaoJiang91/Disease-Progress-Model).

References

1. *The Global Burden of Disease: 2004 Update* (World Health Organization, 2008).
2. Fusar-Poli, P. et al. Heterogeneity of psychosis risk within individuals at clinical high risk: a meta-analytical stratification. *JAMA Psychiatry* **73**, 113–120 (2016).
3. McCutcheon, R. A. et al. The efficacy and heterogeneity of antipsychotic response in schizophrenia: a meta-analysis. *Mol. Psychiatry* **26**, 1310–1320 (2021).
4. Collado-Torres, L. et al. Regional heterogeneity in gene expression, regulation, and coherence in the frontal cortex and hippocampus across development and schizophrenia. *Neuron* **103**, 203–216 (2019).

5. Brugger, S. P. & Howes, O. D. Heterogeneity and homogeneity of regional brain structure in schizophrenia: a meta-analysis. *JAMA Psychiatry* **74**, 1104–1111 (2017).
6. Insel, T. R. & Cuthbert, B. N. Medicine. Brain disorders? Precisely. *Science* **348**, 499–500 (2015).
7. Braff, D. L., Ryan, J., Rissling, A. J. & Carpenter, W. T. Lack of use in the literature from the last 20 years supports dropping traditional schizophrenia subtypes from DSM-5 and ICD-11. *Schizophr. Bull.* **39**, 751–753 (2013).
8. van Erp, T. G. et al. Subcortical brain volume abnormalities in 2,028 individuals with schizophrenia and 2,540 healthy controls via the ENIGMA consortium. *Mol. Psychiatry* **21**, 547–553 (2016).
9. van Erp, T. G. M. et al. Cortical brain abnormalities in 4,474 individuals with schizophrenia and 5,098 control subjects via the Enhancing Neuro Imaging Genetics Through Meta Analysis (ENIGMA) Consortium. *Biol. Psychiatry* **84**, 644–654 (2018).
10. Palaniyappan, L. Progressive cortical reorganisation: a framework for investigating structural changes in schizophrenia. *Neurosci. Biobehav. Rev.* **79**, 1–13 (2017).
11. Alnaes, D. et al. Brain heterogeneity in schizophrenia and its association with polygenic risk. *JAMA Psychiatry* **76**, 739–748 (2019).
12. Jiang, Y. et al. Progressive reduction in gray matter in patients with schizophrenia assessed with MR imaging by using causal network analysis. *Radiology* **287**, 633–642 (2018).
13. Wannan, C. M. J. et al. Evidence for network-based cortical thickness reductions in schizophrenia. *Am. J. Psychiatry* **176**, 552–563 (2019).
14. Jiang, Y. et al. Antipsychotics effects on network-level reconfiguration of cortical morphometry in first-episode schizophrenia. *Schizophr. Bull.* **48**, 231–240 (2022).
15. Kirschner, M. et al. Orbitofrontal-striatal structural alterations linked to negative symptoms at different stages of the schizophrenia spectrum. *Schizophr. Bull.* **47**, 849–863 (2021).
16. Wong, T. Y. et al. An overlapping pattern of cerebral cortical thinning is associated with both positive symptoms and aggression in schizophrenia via the ENIGMA consortium. *Psychol. Med.* **50**, 2034–2045 (2020).
17. Wen, J. et al. Multi-scale semi-supervised clustering of brain images: deriving disease subtypes. *Med. Image Anal.* **75**, 102304 (2022).
18. Lalousis, P. A. et al. Heterogeneity and classification of recent onset psychosis and depression: a multimodal machine learning approach. *Schizophr. Bull.* **47**, 1130–1140 (2021).
19. Chand, G. B. et al. Two distinct neuroanatomical subtypes of schizophrenia revealed using machine learning. *Brain* **143**, 1027–1038 (2020).
20. Yang, Z. et al. A deep learning framework identifies dimensional representations of Alzheimer's disease from brain structure. *Nat. Commun.* **12**, 7065 (2021).
21. Varol, E., Sotiras, A., Davatzikos, C. & Alzheimer's Disease Neuroimaging, I. HYDRA: revealing heterogeneity of imaging and genetic patterns through a multiple max-margin discriminative analysis framework. *Neuroimage* **145**, 346–364 (2017).
22. Dong, A. et al. Heterogeneity of neuroanatomical patterns in prodromal Alzheimer's disease: links to cognition, progression and biomarkers. *Brain* **140**, 735–747 (2017).
23. Dwyer, D. B. et al. Brain subtyping enhances the neuroanatomical discrimination of schizophrenia. *Schizophr. Bull.* **44**, 1060–1069 (2018).
24. Luo, C. et al. Subtypes of schizophrenia identified by multi-omic measures associated with dysregulated immune function. *Mol. Psychiatry* **26**, 6926–6936 (2021).
25. Tronchin, G. et al. Progressive subcortical volume loss in treatment-resistant schizophrenia patients after commencing clozapine treatment. *Neuropsychopharmacology* **45**, 1353–1361 (2020).
26. Young, A. L. et al. Uncovering the heterogeneity and temporal complexity of neurodegenerative diseases with Subtype and Stage iInference. *Nat. Commun.* **9**, 4273 (2018).
27. Vogel, J. W. et al. Four distinct trajectories of tau deposition identified in Alzheimer's disease. *Nat. Med.* **27**, 871–881 (2021).
28. Fillman, S. G. et al. Elevated peripheral cytokines characterize a subgroup of people with schizophrenia displaying poor verbal fluency and reduced Broca's area volume. *Mol. Psychiatry* **21**, 1090–1098 (2016).
29. Li, T. et al. Brain-wide analysis of functional connectivity in first-episode and chronic stages of schizophrenia. *Schizophr. Bull.* **43**, 436–448 (2017).
30. Du, J. et al. The genetic determinants of language network dysconnectivity in drug-naive early stage schizophrenia. *NPJ Schizophr.* **7**, 18 (2021).
31. Crow, T. J. Is schizophrenia the price that *Homo sapiens* pays for language? *Schizophr. Res.* **28**, 127–141 (1997).
32. Palaniyappan, L. & Liddle, P. F. Does the salience network play a cardinal role in psychosis? An emerging hypothesis of insular dysfunction. *J. Psychiatry Neurosci.* **37**, 17–27 (2012).
33. Steen, R. G., Mull, C., McClure, R., Hamer, R. M. & Lieberman, J. A. Brain volume in first-episode schizophrenia: systematic review and meta-analysis of magnetic resonance imaging studies. *Br. J. Psychiatry* **188**, 510–518 (2006).
34. Lieberman, J. A. et al. Hippocampal dysfunction in the pathophysiology of schizophrenia: a selective review and hypothesis for early detection and intervention. *Mol. Psychiatry* **23**, 1764–1772 (2018).
35. Palaniyappan, L. Inefficient neural system stabilization: a theory of spontaneous resolutions and recurrent relapses in psychosis. *J. Psychiatry Neurosci.* **44**, 367–383 (2019).
36. Andreasen, N. C., Liu, D., Ziebell, S., Vora, A. & Ho, B. C. Relapse duration, treatment intensity, and brain tissue loss in schizophrenia: a prospective longitudinal MRI study. *Am. J. Psychiatry* **170**, 609–615 (2013).
37. Austin, S. F. et al. Long-term trajectories of positive and negative symptoms in first episode psychosis: a 10year follow-up study in the OPUS cohort. *Schizophr. Res.* **168**, 84–91 (2015).
38. Galderisi, S., Mucci, A., Buchanan, R. W. & Arango, C. Negative symptoms of schizophrenia: new developments and unanswered research questions. *Lancet Psychiatry* **5**, 664–677 (2018).
39. Addington, J. & Addington, D. Positive and negative symptoms of schizophrenia: their course and relationship over time. *Schizophr. Res.* **5**, 51–59 (1991).
40. Hasan, A. et al. Structural brain changes are associated with response of negative symptoms to prefrontal repetitive transcranial magnetic stimulation in patients with schizophrenia. *Mol. Psychiatry* **22**, 857–864 (2017).
41. Pomponio, R. et al. Harmonization of large MRI datasets for the analysis of brain imaging patterns throughout the lifespan. *Neuroimage* **208**, 116450 (2020).
42. Erikainen, S. & Chan, S. Contested futures: envisioning 'personalized,' 'stratified,' and 'precision' medicine. *New Genet. Soc.* **38**, 308–330 (2019).
43. Liu, Z. et al. Resolving heterogeneity in schizophrenia through a novel systems approach to brain structure: individualized structural covariance network analysis. *Mol. Psychiatry* **26**, 7719–7731 (2021).
44. Wang, L. et al. SchizConnect: mediating neuroimaging databases on schizophrenia and related disorders for large-scale integration. *Neuroimage* **124**, 1155–1167 (2016).

45. Fonteijn, H. M. et al. An event-based model for disease progression and its application in familial Alzheimer's disease and Huntington's disease. *Neuroimage* **60**, 1880–1889 (2012).
46. Lawson, R. G. & Jurs, P. C. New index for clustering tendency and its application to chemical problems. *J. Chem. Inf. Comput. Sci.* **30**, 36–41 (1990).
47. Pan, Y. et al. Morphological profiling of schizophrenia: cluster analysis of MRI-based cortical thickness data. *Schizophr. Bull.* **46**, 623–632 (2020).
48. Sugihara, G. et al. Distinct patterns of cerebral cortical thinning in schizophrenia: a neuroimaging data-driven approach. *Schizophr. Bull.* **43**, 900–906 (2017).
49. Groppe, D. M., Urbach, T. P. & Kutas, M. Mass univariate analysis of event-related brain potentials/fields I: a critical tutorial review. *Psychophysiology* **48**, 1711–1725 (2011).

Acknowledgements

This work was supported by the grant from Science and Technology Innovation 2030-Brain Science and Brain-Inspired Intelligence Project (grant no. 2021ZD0200204 to J.Z.; no. 2022ZD0212800 to Y.T.). This work was supported by National Natural Science Foundation of China (no. 82202242 to Y.J.; no. 82071997 to W.C.; no. 81825009 to W.Y.; no. 82271949 to L.-B.C.; no. 82151314 to J.W.). This work was supported by grants from the National Key R&D Program of China (no. 2022ZD0208500 to D.Y.) and the CAMS Innovation Fund for Medical Sciences (no. 2019-I2M-5-039 to C.L.). This work was supported by the Shanghai Rising-Star Program (no. 21QA1408700 to W.C.) and the Shanghai Sailing Program (22YF1402800 to Y.J.) from Shanghai Science and Technology Committee. This work was supported by the projects from China Postdoctoral Science Foundation (no. BX2021078 and 2021M700852 to Y.J.). This work was supported by National Key R&D Program of China (no. 2019YFA0709502 to J.F.), the grant from Shanghai Municipal Science and Technology Major Project (no. 2018SHZDZX01 to J.F.), ZJ Lab, Shanghai Center for Brain Science and Brain-Inspired Technology, and the grant from the 111 Project (no. B18015 to J.F.). The funders had no role in study design, data collection and analysis, decision to publish or preparation of the manuscript. L.P. acknowledges support from the Monique H. Bourgeois Chair (McGill University) and Tanna Schulich Chair of Neuroscience and Mental Health (Schulich School of Medicine & Dentistry, Western University) and a salary award from the Fonds de recherche du Quebec-Santé (FRQS). We also thank the investigators who provided public access to MRI data from patients diagnosed with schizophrenia through the COBRE database funded by a Center of Biomedical Research Excellence grant 5P20RR021938/P20GM103472 from the NIH to V. Calhoun, the fBIRN data supported by grants to the Function BIRN (U24-RR021992) Testbed funded by the National Center for Research Resources at the National Institutes of Health, USA, the NMorphCH dataset funded by NIMH grant R01MH056584 and the SchizConnect funded by NIMH cooperative agreement 1U01 MH097435. This work is supported by the Zhangjiang International Brain Biobank (ZIB) Consortium.

Author contributions

J.F. led the project. Y.J., W.C. and J.F. were responsible for the study concept and the design of the study. J.W. and E.Z. provided crucial advice for the study. Y.J., E.Z., C.X., W.Z., J.L., D.C., C.S., X.W., B.Z., N.K., Y.-J.S. and J.K. analysed the data and created the figures. Y.J. wrote the manuscript. J.W., E.Z., L.P. and W.C. made substantial contributions to the manuscript and provided critical comments. J.W., E.Z., C. Luo, G.J., J.Y., Y.W., Y.Z., C.-C.H., S.-J.T., X.C., J.Z., H. Huang, H.He, M.D., Y.T., T.Z., C. Li, X.Y., T.S., W.Y., Z.L., L.-B.C., K.W., J.C., C.-P.L. and D.Y. contributed to the data acquisition.

Competing interests

L.P. reports personal fees from Janssen Canada, Otsuka Canada, SPMM Course Limited, UK, Canadian Psychiatric Association; book royalties from Oxford University Press; investigator-initiated educational grants from Janssen Canada, Sunovion and Otsuka Canada outside the submitted work. These interests played no role in the research reported here. Other authors declare no competing interests.

Additional information

Extended data is available for this paper at https://doi.org/10.1038/s44220-023-00024-0.

Supplementary information The online version contains supplementary material available at https://doi.org/10.1038/s44220-023-00024-0.

Correspondence and requests for materials should be addressed to Wei Cheng or Jianfeng Feng.

Peer review information *Nature Mental Health* thanks Johanna Seitz-Holland, Vince Calhoun, Jing Sui and the other, anonymous, reviewer(s) for their contribution to the peer review of this work.

Reprints and permissions information is available at www.nature.com/reprints.

Publisher's note Springer Nature remains neutral with regard to jurisdictional claims in published maps and institutional affiliations.

[1]Institute of Science and Technology for Brain-Inspired Intelligence, Fudan University, Shanghai, China. [2]Key Laboratory of Computational Neuroscience and Brain-Inspired Intelligence(Fudan University), Ministry of Education, Shanghai, China. [3]Shanghai Key Laboratory of Psychotic Disorders, Shanghai Mental Health Center, Shanghai Jiao Tong University School of Medicine, Shanghai, PR China. [4]Peking University Sixth Hospital, Peking University Institute of Mental Health, NHC Key Laboratory of Mental Health (Peking University), National Clinical Research Center for Mental Disorders (Peking University Sixth Hospital), Beijing, PR China. [5]Douglas Mental Health University Institute, Department of Psychiatry, McGill University, Quebec, Quebec, Canada. [6]Robarts Research Institute, University of Western Ontario, London, Ontario, Canada. [7]Lawson Health Research Institute, London, Ontario, Canada. [8]The Clinical Hospital of Chengdu Brain Science Institute, MOE Key Lab for Neuroinformation, School of Life Science and Technology, University of Electronic Science and Technology of China, Chengdu, PR China. [9]High-Field Magnetic Resonance Brain Imaging Key Laboratory of Sichuan Province, Center for Information in Medicine, University of Electronic Science and Technology of China, Chengdu, PR China. [10]Research Unit of NeuroInformation (2019RU035), Chinese Academy of Medical Sciences, Chengdu, PR China. [11]Department of Medical Psychology, Anhui Medical University, Hefei, PR China. [12]National Clinical Research Center for Mental Disorders, Department of Psychiatry, The Second Xiangya Hospital of Central South University, Changsha, PR China. [13]Shanghai Key Laboratory of Brain Functional Genomics (Ministry of Education), Affiliated Mental Health Center (ECNU), School

of Psychology and Cognitive Science, East China Normal University, Shanghai, PR China. [14]Shanghai Changning Mental Health Center, Shanghai, PR China. [15]Department of Psychiatry, Taipei Veterans General Hospital, Taipei, Taiwan. [16]Chinese Institute for Brain Research, Beijing, PR China. [17]PKU-IDG/McGovern Institute for Brain Research, Peking University, Beijing, PR China. [18]Department of Clinical Psychology, Fourth Military Medical University, Xi'an, PR China. [19]Department of Neurology, The First Affiliated Hospital of Anhui Medical University, The School of Mental Health and Psychological Sciences, Anhui Medical University, Hefei, China. [20]Institute of Artificial Intelligence, Hefei Comprehensive National Science Center, Hefei, China. [21]Anhui Province Key Laboratory of Cognition and Neuropsychiatric Disorders, Hefei, China. [22]Collaborative Innovation Center of Neuropsychiatric Disorders and Mental Health, Hefei, China. [23]Anhui Institute of Translational Medicine, Hefei, China. [24]Department of MRI, The First Affiliated Hospital of Zhengzhou University, Zhengzhou, PR China. [25]Institute of Neuroscience, National Yang Ming Chiao Tung University, Taipei, Taiwan. [26]Shanghai Medical College and Zhongshan Hospital Immunotherapy Technology Transfer Center, Shanghai, China. [27]Department of Neurology, Huashan Hospital, Fudan University, Shanghai, China. [28]Fudan ISTBI—ZJNU Algorithm Centre for Brain-Inspired Intelligence, Zhejiang Normal University, Jinhua, China. [29]MOE Frontiers Center for Brain Science, Fudan University, Shanghai, PR China. [30]Zhangjiang Fudan International Innovation Center, Shanghai, PR China. [31]School of Data Science, Fudan University, Shanghai, China. [32]Department of Computer Science, University of Warwick, Coventry, UK. [33]These authors contributed equally: Yuchao Jiang, Jijun Wang, Enpeng Zhou. *A full list of authors and their affiliations appears at the end of the paper. ✉e-mail: wcheng@fudan.edu.cn; jffeng@fudan.edu.cn

the ZIB Consortium

Yuchao Jiang[1,2,33], Xiao Chang[1,2], Chao Xie[1,2], Wei Zhang[1,2], Jinchao Lv[1,2], Di Chen[1,2], Chun Shen[1,2], Xinran Wu[1,2], Bei Zhang[1,2], Nanyu Kuang[1,2], Yun-Jun Sun[1,2], Jujiao Kang[1,2], Jie Zhang[1,2], Wei Cheng[1,2,26,27,28] & Jianfeng Feng[1,2,28,29,30,31,32]

https://doi.org/10.1038/s44220-023-00024-0

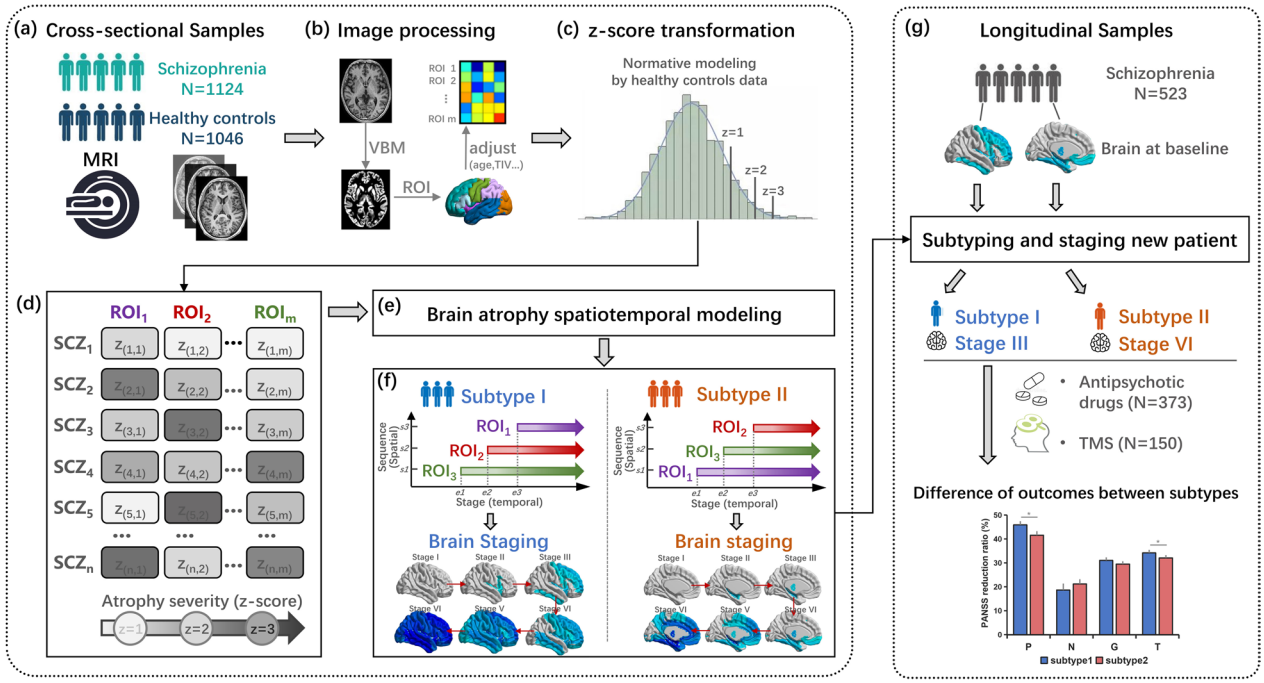

Extended Data Fig. 1 | A flowchart of systematic characterization of heterogeneity in brain atrophy patterning. (a) A total of cross-sectional MRI from 2170 individuals (1124 patients with schizophrenia) was used to characterize heterogeneity in brain atrophy patterning of schizophrenia. **(b)** Brain images were processed using voxel-based morphometry. GMV was extracted from ROIs based on the Automated Anatomical Labeling (AAL) atlas and adjusted by regressing out the effects of sex, age, the square of age, TIV and site effects. **(c)** Adjusted GMV values were normalized relative to control population using *z* scores. Higher *z* scores represent larger deviations from the normal (that is, more severe atrophy in patients with schizophrenia). **(d)** Brain pathophysiological model (that is, SuStaIn [31]) requires both spatial (brain regions) and temporal (*z* scores representing advancing atrophy severity) features as input (that is, an $M \times N$ *z* score matrix). Here, N represents the number of individuals with schizophrenia ($N = 1124$ in this study). M represents the number of ROIs ($M = 17$). **(e)** SuStaIn was used to identify diverse but distinct patterns of progression using cross-sectional neuroimaging data and to cluster individuals while accounting for disease progression. **(f)** Individuals with schizophrenia were classified according to the sequence of atrophy in different brain regions. For each subtype, brain-based staging was assessed from progressive spatial patterns with distinct origins. **(g)** Using a longitudinal sample, we examined whether subtype classification based on baseline brain features predict differential treatment response to antipsychotic medications and TMS.

https://doi.org/10.1038/s44220-023-00024-0

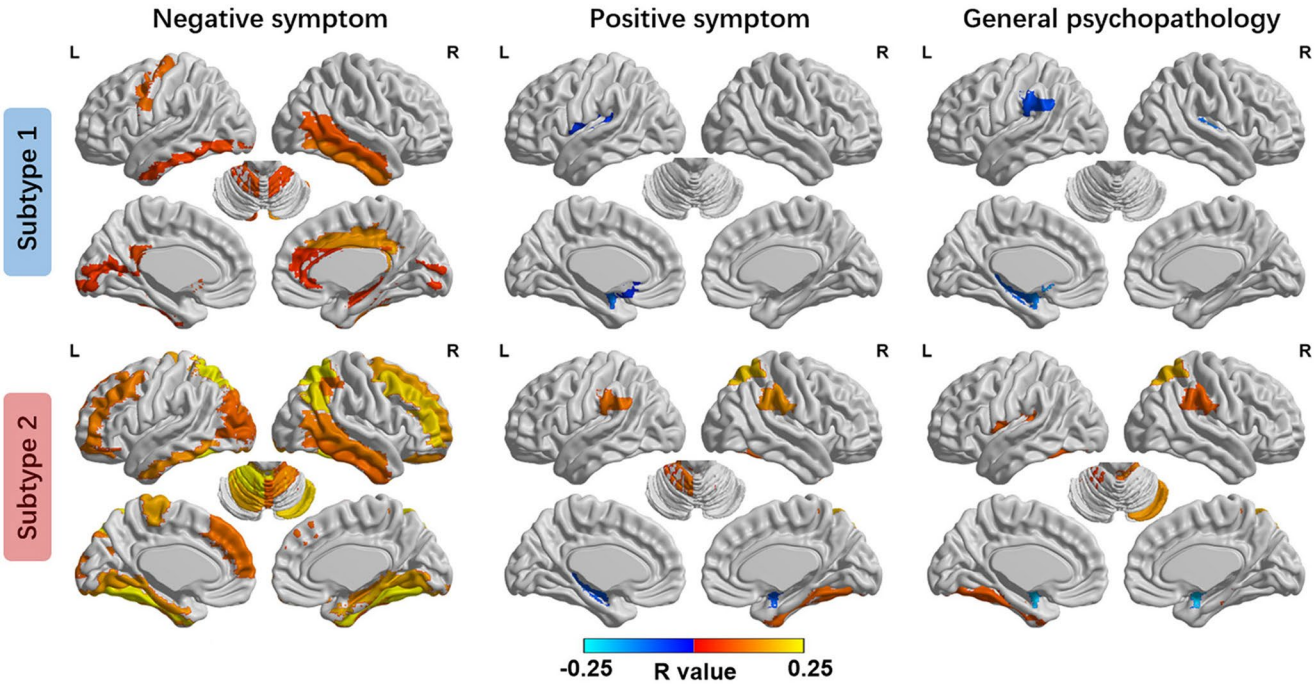

Extended Data Fig. 2 | Association between regional atrophy and clinical symptoms. Spearman correlation analysis between PANSS (positive, negative and general psychopathology subscales) and GMV *z* scores were performed after adjusting for sex, age, the square of age, TIV and sites. Colored bar represents the r value after controlling the FWE corrected $P < 0.05$. L, left hemisphere; R, right hemisphere.

nature portfolio

Corresponding author(s): Jianfeng Feng, Wei Cheng

Last updated by author(s): Dec 17, 2022

Reporting Summary

Nature Portfolio wishes to improve the reproducibility of the work that we publish. This form provides structure for consistency and transparency in reporting. For further information on Nature Portfolio policies, see our Editorial Policies and the Editorial Policy Checklist.

Statistics

For all statistical analyses, confirm that the following items are present in the figure legend, table legend, main text, or Methods section.

n/a	Confirmed
☐	☒ The exact sample size (*n*) for each experimental group/condition, given as a discrete number and unit of measurement
☐	☒ A statement on whether measurements were taken from distinct samples or whether the same sample was measured repeatedly
☐	☒ The statistical test(s) used AND whether they are one- or two-sided *Only common tests should be described solely by name; describe more complex techniques in the Methods section.*
☐	☒ A description of all covariates tested
☐	☒ A description of any assumptions or corrections, such as tests of normality and adjustment for multiple comparisons
☐	☒ A full description of the statistical parameters including central tendency (e.g. means) or other basic estimates (e.g. regression coefficient) AND variation (e.g. standard deviation) or associated estimates of uncertainty (e.g. confidence intervals)
☐	☒ For null hypothesis testing, the test statistic (e.g. *F*, *t*, *r*) with confidence intervals, effect sizes, degrees of freedom and *P* value noted *Give P values as exact values whenever suitable.*
☐	☒ For Bayesian analysis, information on the choice of priors and Markov chain Monte Carlo settings
☒	☐ For hierarchical and complex designs, identification of the appropriate level for tests and full reporting of outcomes
☒	☐ Estimates of effect sizes (e.g. Cohen's *d*, Pearson's *r*), indicating how they were calculated

Our web collection on statistics for biologists contains articles on many of the points above.

Software and code

Policy information about availability of computer code

Data collection	T1-weighted images were processed using the Computational Anatomy Toolbox (version: r1720) (http://www.neuro.uni-jena.de/cat/) within SPM12 (https://www.fil.ion.ucl.ac.uk/spm/software/spm12/). A fully automated procedure for standard voxel-based morphometry (VBM) was conducted to result in gray matter volume (GMV) images. Mean GMV values within different regions of interest (ROIs) were extracted for each subject using AAL atlas.
Data analysis	Subtype and Stage Inference (SuStaIn) was the central algorithm to perform disease progression modeling in this manuscript. The SuStaIn has been described previously (Young et al 2018 Nature Communications) and Python codes are available on GitHub (https://github.com/ucl-pond/pySuStaIn). The visualization of ROI-wise z-score images was conducted using BrainNetViewer (https://www.nitrc.org/projects/bnv/). All other analyses, including correlation analysis, t-test, ANOVA were conducted using MATLAB R2018b.

For manuscripts utilizing custom algorithms or software that are central to the research but not yet described in published literature, software must be made available to editors and reviewers. We strongly encourage code deposition in a community repository (e.g. GitHub). See the Nature Portfolio guidelines for submitting code & software for further information.

Data

Policy information about availability of data

All manuscripts must include a data availability statement. This statement should provide the following information, where applicable:

- Accession codes, unique identifiers, or web links for publicly available datasets
- A description of any restrictions on data availability
- For clinical datasets or third party data, please ensure that the statement adheres to our policy

Data of COBRE, NMorphCH, FBIRN and NUSDAST were obtained from the SchizConnect, a publicly available website (http://www.schizconnect.org/documentation#by_project). The NMorphCH dataset and NUSDAST dataset were download through a query interface at the SchizConnect (http://www.schizconnect.org/queries/new). The COBRE dataset was download from the Center for Biomedical Research Excellence in Brain Function and Mental Illness (COBRE) (https://coins.trendscenter.org/). The FBIRN dataset was download from https://www.nitrc.org/projects/fbirn/. The DS000115 dataset was download from OpenfMRI database (https://www.openfmri.org/). Data from the other datasets (cross-sectional datasets #1, #2, #3, #4, longitudinal AMP and TMS data) are not publicly available for download, but access requests can be made to the respective study investigators: cross-sectional data (dataset #1, #2, #3, #4) -- J.Feng; APM data -- J.Wang, X.Yu, W.Yue and C.Luo; TMS data -- J.Wang, G.Ji, L.Cui and C.Luo. Requests for raw and analyzed data can be made to the corresponding author (J.Feng, jffeng@fudan.edu.cn) and will be promptly reviewed by the Fudan University Ethics Committee to verify whether the request is subject to any intellectual property or confidentiality obligations.

Human research participants

Policy information about studies involving human research participants and Sex and Gender in Research.

Reporting on sex and gender	Term 'sex' was used due to the biological attribution. The sex was determined based on self-reporting. Cross-sectional sample included 1124 individuals with schizophrenia (479 females, age=31.1±12.8 years) and 1046 healthy subjects (498 females, age=32.6±12.4 years). APM sample included 373 patients with schizophrenia (190 females, age=26.4±9.0 years). TMS sample included 150 patients with schizophrenia (66 females, age=30.1±12.3 years).
Population characteristics	This information is provided in detail in Table S1 and Supplementary Materials, but for a summary: Cross-sectional sample included 1124 individuals with schizophrenia (479 females, age=31.1±12.8 years) and 1046 healthy subjects (498 females, age=32.6±12.4 years). APM sample included 373 patients with schizophrenia (190 females, age=26.4±9.0 years). TMS sample included 150 patients with schizophrenia (66 females, age=30.1±12.3 years).
Recruitment	Most of subjects were recruited from four local mental hospital or general hospital, each with academic centers. Patients with schizophrenia were diagnosed according to the Diagnostic and Statistical Manual of Mental Disorders, 4th Edition (DSM-IV). Individuals were excluded from the study if they were (1) diagnosed with schizoaffective disorder, mood disorders, or other major medical or neurologic disorders; (2) alcohol/drug dependence; (3) had a history of electroconvulsive therapy within six months; (4) other contraindications to MRI scanning. These patients were mainly from relatively developed cities in China (such as provincial capitals or regional central cities), which may have potential regional bias. Due to the requirement of MRI scanning after enrollment, patient compliance may be a bias that affects the final enrollment outcome. Data from open databases (COBRE, NMorphCH, FBIRN, NUSDAST, DS000115) are from several centers, each with their own recruitment parameters (www.schizconnect.org). Overall, such a sample has the advantage of covering a wide population of schizophrenia cases from many parts of the world. Written informed consent was obtained from all participants and/or their legal guardians. Participants received travel compensation and remuneration up to 300 Chinese Yuan based on the study they participated in.
Ethics oversight	The study has been approved by the Medical Research Ethics Committees of the local hospitals (ethics number: 2017-36R[dataset#1], 2018-KY-88[dataset#2], YM105091F[dataset#3], CDFH2014030501[dataset#4], 2017-36R[Shanghai], 2008-2[Beijing1], 2017-16[Beijing2], CDFH2014030501[Chengdu], 2016003[Anhui], XJYYLL-2015047[Xi'an] and IRB2019-004[Harbin]).

Note that full information on the approval of the study protocol must also be provided in the manuscript.

Field-specific reporting

Please select the one below that is the best fit for your research. If you are not sure, read the appropriate sections before making your selection.

☒ Life sciences ☐ Behavioural & social sciences ☐ Ecological, evolutionary & environmental sciences

For a reference copy of the document with all sections, see nature.com/documents/nr-reporting-summary-flat.pdf

Life sciences study design

All studies must disclose on these points even when the disclosure is negative.

Sample size	Because comprehensive effect size/power calculations have not been comprehensively investigated for SuStaIn, the sample size was determined according to previous SuStaIn studies (Young et al., 2018, Nature Communications and Vogel et al., 2021, Nature Medicine).As

these previous studies indicated that about 30-40% subjects would actually exhibit measurable abnormal gray matter volume reductions. For this reason, it was important for us to analyze data from at least 600 patients with schizophrenia, and ideally greater than 1000. The sample size for this study is over 2000 participants (over 1000 patients with schizophrenia), which gives us broad representation across the disease progress for SuStaIn modeling. Cross-sectional between-group comparisons included 631 participants for subtype1 and 493 participants for subtype2. Longitudinal between-group comparisons included a minimum of 150 participants, which provides sufficient power to detect clinically relevant effect sizes for between-group comparisons.

Data exclusions

Individuals were excluded from the study if they were (1) diagnosed with schizoaffective disorder, mood disorders, or other major medical or neurologic disorders; (2) alcohol/drug dependence; (3) had a history of electroconvulsive therapy within six months; (4) other contraindications to MRI scanning.
As the samples included multi-center data with possibly large variation, it is important to conduct a protocol to ensure data quality. The data quality control (QC) steps are described as follows: (1) QC for raw T1-weighted images. Raw T1-weighted structural brain images were checked for large distortions, ghosting or other abnormalities by at least two experienced neuroradiologists. (2) QC for image processing. Raw T1-weighted structural brain images were processed with the Computational Anatomy Toolbox (CAT) within SPM (http://www.neuro.uni-jena.de/cat/). The results of segment and spatial normalization were visually inspected by at least two experienced specialists in brain image processing. (3) After data processing, CAT reported a weighted average image quality rating (IQR>3) to exclude those subjects with poor quality. These quality control steps allowed us to exclude those subjects with poor quality and generate a subject list for the following analysis.

Replication

To evaluate the consistency of the SuStaIn model, we used 2-fold cross-validation method.
The cohort was randomly split into two non-overlapping subfolds (50% of the subjects as one subfold and left 50% as the other subfold). This procedure was repeated ten times to avoid the occasionality of one split. For each non-overlapping subfold, the SuStaIn model was trained on one of non-overlapping folds, and further tested using the other non-overlapping subfold. To establish the SuStaIn validity for an alternative atlas, another three commonly used atlases (BN246 atlas, Schaefer200 atlas, and HCPMMP360 atlas) were applied for ROI extraction and SuStaIn modelling. To evaluate the stability of SuStaIn at a relative higher spatial resolution, the 17 AAL features were expand to 22 and 27 features (AAL22 and AAL27) by a data-driven hierarchical clustering procedure. A total of five validation sets of features were generated to further verify the stability of SuStaIn. In addition, we also examined the stability of SuStaIn 'trajectories' using leave one-site out resampling.

Randomization

This is not relevant because we did not conduct a controlled trial. Rather, we combined individuals with schizophrenia from several cohorts, and conducted a data-driven algorithm to subtyping. We further compared demographic and disease features between subtypes.

Blinding

Blinding was not relevant for experiments because SuStaIn is a data-driven method without the needs of demographic or clinical data. Co-authors who collected the demographic and clinical information of individuals were blinded to the SuStaIn subtyping results. Co-authors who performed the data preprocessing were blinded to the demographic and clinical information of individuals. Therefore, while the researchers were not blinded, the analysis effectively was.

Reporting for specific materials, systems and methods

We require information from authors about some types of materials, experimental systems and methods used in many studies. Here, indicate whether each material, system or method listed is relevant to your study. If you are not sure if a list item applies to your research, read the appropriate section before selecting a response.

Materials & experimental systems

n/a	Involved in the study
☒	☐ Antibodies
☒	☐ Eukaryotic cell lines
☒	☐ Palaeontology and archaeology
☒	☐ Animals and other organisms
☐	☒ Clinical data
☒	☐ Dual use research of concern

Methods

n/a	Involved in the study
☒	☐ ChIP-seq
☒	☐ Flow cytometry
☐	☒ MRI-based neuroimaging

Clinical data

Policy information about clinical studies

All manuscripts should comply with the ICMJE guidelines for publication of clinical research and a completed CONSORT checklist must be included with all submissions.

Clinical trial registration

ChiCTR2000041106

Study protocol

http://www.chictr.org.cn/showprojen.aspx?proj=65566

Data collection

Patients with first-episode schizophrenia who agreed to receive repeated TMS (rTMS) and signed the informed consent were recruited from Harbin First Specialized Hospital. PANSS and MRI data were collected at baseline and 4 weeks follow-up.
Recruiting time: From 2019-11-05 To 2021-12-08
Study execute time: From 2019-11-05 To 2022-12-08

Outcomes

Outcomes is clinical symptom assessment that was assessed using the Positive and Negative Syndrome Scale (PANSS) and neuroimaging biomarker that was measured by MRI scanning.

Magnetic resonance imaging

Experimental design

Design type	This is not relevant because subjects did not need to perform experiment.
Design specifications	This is not relevant because subjects did not need to perform experiment.
Behavioral performance measures	This is not relevant because subjects did not need to perform experiment.

Acquisition

Imaging type(s)	structural
Field strength	3T
Sequence & imaging parameters	3-Tesla MRI scanner (Siemens MR B17) was used to acquire data in Dataset#1. High-spatial-resolution T1-weighted images were collected by a magnetization-prepared rapid acquisition gradient echo (MPRAGE) sequence. The main parameters included repetition time/echo time, 2530/2.56 msec; flip angle, 7°; field of view, 256 × 256 mm2; matrix size, 256 × 256; section thickness, 1 mm (no gap); and voxel size, 1×1×1mm3. 3-Tesla GE Discovery MR750 scanner (General Electric, Fairfield Connecticut, USA) was used to acquire data in Dataset#2. Structural T1-weighted images were scanned with 3D spoiled gradient echo scan sequence: Repetition time = 8164 ms, echo time = 3.18 ms, inversion time = 900 ms, flip angle = 7°, resolution matrix = 256 × 256, slices =188, thickness = 1.0 mm, and voxel size = 1×1×1 mm3. 3T MR system (Siemens Magnetom Tim Trio, Erlangen, Germany) at Dataset#3, equipped with a high-resolution 12-channel head array coil. A high-resolution anatomical T1-weighted image was acquired with sagittal 3D magnetization-prepared rapid gradient echo (MPRAGE) sequence: repetition time (TR) = 3500 ms, echo time (TE) = 3.5 ms, inversion time = 1100 ms, flip angle = 7°, field of view (FOV) = 256 mm × 256 mm, 192 slices, slice thickness = 1 mm, voxel size =1.0 mm × 1.0 mm × 1.0 mm. 3-Tesla MRI scanner (GE DISCOVERY MR 750, USA) was used to collect imaging data in Dataset#4. High-resolution T1-weighted images were acquired using a three dimensional fast spoiled gradient echo (T1-3D FSPGR) sequence. The main parameters include: TR = 6.008 ms; TE = 1.984 ms; flip angle (FA) =9°; field of view (FOV) = 25.6 cm × 25.6 cm; matrix size = 256 × 256; slice thickness = 1 mm (no gap). Scanning parameters of datasets(COBRE, NMorphCH, FBIRN, NUSDAST) are described in website (www.schizconnect.org). Scanning parameters of datasets(DS000115) are described in website (https://www.openfmri.org/dataset/ds000115/).
Area of acquisition	whole brain scan

Diffusion MRI ☐ Used ☒ Not used

Preprocessing

Preprocessing software	T1-weighted images were processed using the Computational Anatomy Toolbox (http://www.neuro.uni-jena.de/cat/) within SPM12 (https://www.fil.ion.ucl.ac.uk/spm/software/spm12/). A fully automated procedure for standard voxel-based morphometry (VBM) (including spatial registration, tissue segmentation and bias correction of intensity non-uniformities) was conducted, resulting in gray matter volume (GMV) images.
Normalization	VBM procedures including spatial registration, tissue segmentation and bias correction of intensity non-uniformities were conducted using CAT12.
Normalization template	VBM procedures including spatial registration, tissue segmentation and bias correction of intensity non-uniformities were conducted using CAT12 (http://dbm.neuro.uni-jena.de/cat/index.html#VBM).
Noise and artifact removal	VBM procedures including spatial registration, tissue segmentation and bias correction of intensity non-uniformities were conducted using CAT12.
Volume censoring	VBM procedures including spatial registration, tissue segmentation and bias correction of intensity non-uniformities were conducted using CAT12.

Statistical modeling & inference

Model type and settings	A novel data-driven approach – Subtype and Stage Inference (SuStaIn) was used to perform disease progression modeling and cluster individuals while accounting for disease progression. The SuStaIn has been described previously (Young et al 2018 Nature Communications).
Effect(s) tested	This is not relevant because this study is a structural MRI study rather than task fMRI.

Specify type of analysis: ☐ Whole brain ☒ ROI-based ☐ Both

Anatomical location(s)	The GMV images were parcellated based on the automated anatomical (AAL) atlas. These parcellations were used to extract mean GMV values within different regions of interest (ROIs) for each subject.
Statistic type for inference (See Eklund et al. 2016)	This is not relevant because GMV value was extracted at ROI-level.
Correction	FWE, FDR

Models & analysis

n/a	Involved in the study
☒	☐ Functional and/or effective connectivity
☒	☐ Graph analysis
☒	☐ Multivariate modeling or predictive analysis